

1 African Swine Fever Virus and host response - transcriptome
2 profiling of the Georgia 2007/1 strain and porcine macrophages

3

4 Gwenny Cackett^{a§}, Raquel Portugal^{b§}, Dorota Matelska^a, Linda Dixon^{b#} and Finn Werner^{a#}

5 ^aInstitute for Structural and Molecular Biology, Darwin Building, University College London, Gower
6 Street, London WC1E 6BT, United Kingdom

7 ^bPirbright Institute, Ash Road, Pirbright, Surrey, GU24 0NF, United Kingdom

8 [§] have contributed equally to this work

9

10 Short Title:

11 The ASFV Georgia 2007/1 Strain Transcriptome

12 #Address correspondence to Linda Dixon, linda.dixon@pirbright.ac.uk, or Finn Werner,

13 f.werner@ucl.ac.uk.

14 Abstract [222 words]

15 African swine fever virus (ASFV) has a major global economic impact. With a case fatality in domestic
16 pigs approaching 100%, it currently presents the largest threat to animal farming. Although genomic
17 differences between attenuated and highly virulent ASFV strains have been identified, the molecular
18 determinants for virulence at the level of gene expression have remained opaque. Here we
19 characterise the transcriptome of ASFV genotype II Georgia 2007/1 (GRG) during infection of the
20 physiologically relevant host cells, porcine macrophages. In this study we applied Cap Analysis Gene
21 Expression sequencing (CAGE-seq) to map the 5' ends of viral mRNAs at 5 and 16 hours post-infection.
22 A bioinformatics analysis of the sequence context surrounding the transcription start sites (TSSs)
23 enabled us to characterise the global early and late promoter landscape of GRG. We compared
24 transcriptome maps of the GRG isolate and the lab-attenuated BA71V strain that highlighted GRG
25 virulent-specific transcripts belonging to multigene families, including two predicted MGF 100 genes
26 I7L and I8L. In parallel, we monitored transcriptome changes in the infected host macrophage cells.
27 Of the 9,384 macrophage genes studied, transcripts for 652 host genes were differentially regulated
28 between 5 and 16 hours-post-infection compared with only 25 between uninfected cells and 5 hours
29 post-infection. NF- κ B activated genes and lysosome components like S100 were upregulated, and
30 chemokines such as CCL24, CXCL2, CXCL5 and CXCL8 downregulated.

31 Importance [183 words]

32 African swine fever virus (ASFV) causes haemorrhagic fever in domestic pigs with case fatality rates
33 approaching 100%, and no approved vaccines or antivirals. The highly-virulent ASFV Georgia 2007/1
34 strain (GRG) was the first isolated when ASFV spread from Africa to the Caucasus region in 2007. Then
35 spreading through Eastern Europe, and more recently across Asia. We used an RNA-based next
36 generation sequencing technique called CAGE-seq to map the starts of viral genes across the GRG DNA
37 genome. This has allowed us to investigate which viral genes are expressed during early or late stages
38 of infection and how this is controlled, comparing their expression to the non-virulent ASFV-BA71V
39 strain to identify key genes that play a role in virulence. In parallel we investigated how host cells
40 respond to infection, which revealed how the ASFV suppresses components of the host immune
41 response to ultimately win the arms race against its porcine host.

42 Introduction [1,317 words]

43 ASFV originated in Sub-Saharan Africa where it remains endemic. However, following the introduction
44 in 2007, of a genotype II isolate to Georgia (1), and subsequent spread in Russia and Europe. The virus

45 was then introduced to China in 2018 (2), from here it spread rapidly across Asia, strongly emphasizing
46 this disease as a severe threat to global food security. ASFV is the only characterised member of the
47 Asfarviridae family (3) in the recently classified Nucleocytoviricota (ICTV Master Species List 2019.v1)
48 phylum (4,5). ASFV has a linear double-stranded DNA (dsDNA) genome of ~170–193 kbp encoding
49 ~150–~200 open reading frames (ORFs). Until recently, little was known about either the transcripts
50 expressed from the ASFV genome or the mechanisms of ASFV transcription. Much of what is known
51 about transcription is extrapolated from vaccinia virus (VACV), a distantly-related Nucleocytoviricota
52 member, from the Poxviridae family (6). ASFV encodes a eukaryotic-like 8-subunit RNA polymerase
53 (RNAP), an mRNA capping enzyme and poly-A polymerase, all of which are carried within mature virus
54 particles (7). These virions are transcription competent upon solubilisation in vitro (8) and support
55 mRNA modification by including a 5'-methylated cap and a 3' poly-adenylated (polyA) tail of ~33
56 nucleotide-length (8,9).

57 Viral genes are typically classified according to their temporal expression patterns - ASFV genes have
58 historically been categorised as 'immediate early' when expressed immediately following infection, as
59 'early genes' following the onset of viral protein synthesis, as 'intermediate genes' after the onset of
60 viral DNA replication, or as 'late genes' thereafter. The temporal regulation of transcription is likely
61 enabled by different sets of general transcription initiation factors that recognise distinct early or late
62 promoter motifs (EPM or LPM, respectively), as we previously investigated in the ASFV-BA71V strain
63 (10), and address further in this study. EPM recognition is likely enabled by the ASFV homologue of
64 heterodimeric VACV early transcription factor (VETF), consisting of D1133L (D6) and G1340L (A7) gene
65 products, which bind the Poxvirus early gene promoter motif (11–13), which the ASFV EPM strongly
66 resembles. Both ASFV-D6 and ASFV-A7 are late genes, i.e. synthesised late during infection (10) and
67 packaged into virus particles (7). The ASFV LPM is less well defined than the EPM, but a possible
68 initiation factor involved in its recognition is the ASFV-encoded viral homolog of the eukaryotic TATA-
69 binding protein (TBP), expressed during early infection (10). By analogy with the VACV system,
70 additional factors including homologs of A1, A2 and G8 may also contribute to late transcription
71 initiation (6)

72 We have recently carried out a detailed and comprehensive ASFV whole genome expression analysis
73 using complimentary next-generation sequencing (NGS) results and computational approaches to
74 characterise the ASFV transcriptome following BA71V infection of Vero cells at 5 hpi and 16 hpi post-
75 infection (hpi) (10). Most of our knowledge about the molecular biology of ASFV, including gene
76 expression, has been derived from cell culture-adapted, attenuated virus strains, such as BA71V
77 infecting Vero tissue culture cells (9,10). These model systems provide convenient models to study

78 the replication cycle but have deletions of many genes that are not essential for replication, but have
79 important roles in virulence within its natural porcine hosts. (14–16). To date 24 ASFV genotypes have
80 been identified in Africa (16–23), while all strains spreading across Asia and Europe belong to the Type
81 II genotype. Most of these are highly virulent in domestic pigs and wild boar, including the ASFV
82 Georgia 2007/1 (GRG) (24), and the Chinese ASFV Heilongjiang, 2018 (Pig/HLJ/18) (25) isolates.
83 Though a number of less virulent isolates have been identified in wild boar in the Baltic States and
84 domestic pigs in China (26–29). It is crucial to understand the similarities and commonalities between
85 ASFV strains, and to characterise the host response to these in order to understand the molecular
86 determinants for ASFV pathogenicity. Information about the gene content and genome organisation
87 can be gained from comparing virus genome sequences. However, only functional genomics such as
88 transcriptome or proteome analyses can provide information about the differences in gene expression
89 programmes and the host responses to infection.

90 On the genome level, most differences between virulent (e.g. GRG) and attenuated (e.g. lab-
91 attenuated BA71V) ASFV strains reside towards the genome termini. Figure 1a shows a whole genome
92 comparison of GRG (left) and BA71V (right) strains with the sequence conservation colour coded in
93 different shades of blue. The regions towards the ends of the genome are more dynamic compared to
94 the central region which is highly conserved, as genes at the termini are prone to deletion, duplication,
95 insertion, and fusion (17,30). Most of the GRG-specific genes are expressed early during infection
96 (early genes are colour coded blue in the outer arch of Figure 1a) and many belong to Multi-Gene
97 Families (MGFs, purple in the inner arch). The functions of many MGF members remain poorly
98 understood, though variation among MGFs is linked to virulence (31) and deleting members of MGF
99 360 and 505 families has been shown to reduce virulence (32,33). Deletion of MGF 505-7R or MGF
100 110-9L also partially attenuated the virus in pigs (34,35). In contrast deletion of MGF 110-1L and MGF
101 100-1R did not reduce virus virulence (17). Members of MGF 110 are highly expressed both on the
102 mRNA and protein level in infections with the BA71V isolate or OURT88/3 (10,36), suggesting MGF
103 110 holds importance during infection. Overall, the functions of MGF 360 and 505 members are better
104 characterised than other MGFs, playing a role in evading the host type I interferon (IFN) response
105 (15,32,37–40). In summary, comparing the expression of ASFV genes, especially MGFs, between the
106 virulent GRG- and the lab adapted BA71V strains, is fundamental in identification of virulence factors
107 and better MGF characterisation.

108 Macrophages are the primary target cells for ASFV, they are important immune effector cells that
109 display remarkable plasticity allowing efficient response to environmental signals (41). There are
110 some studies which have investigated how host macrophages respond to infection, including a

111 microarray analysis of primary swine macrophage cells infected with virulent GRG (42). There are two
112 RNA-seq studies of whole blood or tissues isolated from pigs post-mortem, which were infected with
113 either a low pathogenic ASFV-OURT 88/3 or ASFV-GRG (43), or infected with a pathogenic Chinese
114 isolate ASFV-SY18 (44). Recently, two reports have been published about the transcriptomic response
115 of porcine macrophages to infection with a virulent Chinese genotype II isolate using a low multiplicity
116 of infection (MOI: 1) and classical RNA-seq (45,46), but due to different experimental conditions the
117 varying results are somewhat challenging to compare with other studies. It must also be remembered
118 that neither these classical RNA-seq nor microarray analyses, have sufficient resolution to accurately
119 capture viral gene expression in the compact ASFV genome alongside that of the host.

120 Here we applied CAGE-seq to characterise the transcriptome of the highly virulent GRG isolate (24),
121 in primary porcine macrophages, the biologically relevant target cells for ASFV infection. In this study
122 we used a high multiplicity of infection (MOI: 5), so that transcripts expressed during a single cycle
123 time course could be measured without the complication of variable proportions of uninfected cells
124 being present. We investigated the differential gene expression patterns of viral mRNAs at early and
125 late time points of 5- and 16 hpi, and mapped the viral promoter motifs. Importantly, we have
126 compared the expression levels and temporal regulation of genes conserved in both the virulent GRG
127 isolate, and attenuated tissue-culture adapted BA71V strain. With a few exceptions, both mRNA
128 expression levels and temporal regulation of the conserved genes are surprisingly similar. This
129 confirms that it is not deregulation of their conserved genes, but the virulent isolate-specific genes,
130 which are the key determinants for ASFV virulence. Most of these genes are MGF members, likely
131 involved in suppression of the host immune-response. Indeed, transcriptome analysis of the porcine
132 macrophages upon GRG infection reflects a modulation of host immune response genes, although the
133 bulk of the ~ 9000 genes studied did not significantly change expression levels during infection.

134 Results [4,633 words]

135 Genome-wide Transcription Start Site-Mapping

136 We infected primary porcine alveolar macrophages with ASFV GRG at a high multiplicity of infection
137 (MOI 5.0), isolated total RNA at 5 hpi and 16 hpi and sequenced using CAGE-seq (Supplementary Table
138 1a). The resulting mRNA 5' ends were mapped to the GRG genome (Figure 1b) resulting in the
139 annotation of 229 and 786 TSSs at 5 and 16 hpi, respectively (Figure 1c and d, from Supplementary
140 Table 1b and c, respectively). The majority of TSSs were identified within 500 bp upstream of the start
141 codon of a given ORF, a probable location for a *bona fide* gene TSS. The strongest and closest TSSs
142 upstream of ORFs were annotated as 'primary' TSS (pTSS, listed in Supplementary Table 1d) and in this

143 manner we could account TSS for 177 out of 189 GRG ORFs annotated in the FR682468.1 genome.
144 TSSs signals below the threshold for detection included MGF_110-11L, C62L, and E66L, the remainder
145 being short ORFs designated as 'ASFV_G_ACD', predicted solely from the FR682468 genome sequence
146 (24). The E66L ORF was originally predicted from only the BA71V genome sequence, but likewise was
147 undetectable with CAGE-seq (10), making its expression unlikely. Our TSS mapping identified novel
148 ORFs (nORFs) downstream of the TSS, which were included in the curated GRG genome map
149 (Supplementary Table 1d includes pTSSs of annotated ORFs and nORFs in gene feature file or 'GFF'
150 format). In addition to ORF-associated TSSs, some were located within ORFs (intra-ORF or ioTSS), or
151 in between them (inter-ORF TSS), and all detected TSSs are listed in Supplementary Table 1b-c.

152 Expression of GRG genes during Early and Late Infection

153 Having annotated TSSs across the GRG genome, we quantified the viral mRNAs originating from pTSSs
154 from CAGE-seq data, normalising against the total number of reads mapping to the ASFV genome (i.
155 e. RPM or reads per million mapped reads per sample). We compared gene expression between early
156 and late infection, and simplistically defined genes as 'early' or 'late' if they are significantly down- or
157 upregulated (respectively), using DESeq2 (47). In summary, 165 of the 177 detectable genes were
158 differentially expressed (adjusted p-value or padj < 0.05, Supplementary Table 1e). Those showing no
159 significant change were D345L, DP79L, I8L, MGF_100-1R, A859L, QP383R, B475L, E301R, DP63R,
160 C147L, and I177L. 87 of those 165 differentially expressed genes were significantly downregulated,
161 thus representing the 'early genes', while 78 of the 165 genes were upregulated or 'late genes'. The
162 majority of MGFs were early genes, apart from MGF 505-2R, MGF 360-2L and MGF 100-1L (Figure 2a).
163 Figure 2b shows the expression patterns of GRG-exclusively expressed genes, which we defined as
164 only having a detectable CAGE-seq TSS in GRG, and not in BA71V (regardless of presence in the BA71V
165 genome). These unsurprisingly, consist of many MGFs (19), all of which were early genes (Figure 2b),
166 barring MGF 100-1L. In addition genes I9R, I10L and I11L and several of the newly annotated short
167 ORFs were specific to GRG.

168 We extracted the top twenty most highly expressed genes of GRG (as RPM) during 5 hpi (Figure 2c)
169 and 16 hpi (Figure 2d) post-infection. Ten genes are shared between both top 20 lists: MGF 110-3L,
170 A151R, MGF 110-7L, MGF 110-5L-6L, I73R, 285L, CP312R, ASFV_G_ACD_00600, MGF 110-4L, and
171 CP204L. It is important to note that the relative expression values (RPM) for genes at 5 hpi are
172 significantly higher than those at 16 hpi. This is consistent with our observations in the BA71V strain
173 (10) and due to the increase in global viral transcript levels during late infection discussed below.
174 Supplementary Table 1f includes all the GRG annotated ORFs, their TSS locations during early and late

175 infection, their relative distances if these TSS locations differ, and their respective 5' Untranslated
176 Region (UTR) lengths.

177 GRG and BA71V Share Strong Similarity between Conserved Gene Expression

178 Next we carried out a direct comparison of mRNA levels from 132 conserved genes between the
179 virulent GRG and attenuated BA71V (10) strain making use of our previously published CAGE-seq data.
180 The relative transcript levels (RPM) of the genes conserved between the two strains showed a
181 significant correlation at 5 hpi (Figure 3a) and 16 hpi (Figure 3b), supported by the heatmap in
182 Supplementary Figure 1, the RPM for each gene, across both time-points and replicates, showing a
183 strong congruence between the two strains. Of the 132 conserved genes, 125 showed significant
184 differential expression in both strains. 119 of these 125 showed the same down- or up-regulated
185 patterns of significant differential expression from 5 hpi to 16 hpi (Figure 3c, early genes in blue, late
186 genes in red). The exceptions are D205R, CP80R, C315R, NP419L, F165R, and DP148R (MGF 360-18R),
187 encoding RNA polymerase subunits RPB5 and RPB10 (15), Transcription Factor IIB (TFIIB) (15), DNA
188 ligase (48), a putative signal peptide-containing protein, and a virulence factor (49), respectively. The
189 ASFV-TFIIB homolog (C315R) is classified as an early gene in GRG but not in BA71V, in line with the
190 predominantly early-expressed TBP (B263R), its predicted interaction partner. It is worth noting
191 however, that D205R, CP80R, and C315R are close to the threshold of significance, with transcripts
192 being detected at both 5 hpi and 16 hpi (Supplementary Table 1e).

193 Increased and pervasive transcription during late infection

194 During late infection of BA71V (10), we noted an increase in genome-wide mRNA abundance, as well
195 as an increasing number of TSSs and transcription termination sites, reminiscent of pervasive
196 transcription observed during late infection of Vaccinia virus (50). To quantify and compare the global
197 mRNA increase both in BA71V and GRG, we calculated the ratio of read coverage per nucleotide, at
198 16 hpi versus 5 hpi (\log_2 transformed ratio of RPM), across the viral genome (Figure 4a, increase shown
199 above- and decrease below the x-axis). This dramatic increase is due to the overall increase of virus
200 mRNAs present, which is visible in both strains (Figure 4b), with a ~2 fold increase in GRG from 5 hpi
201 to 16 hpi, versus ~8 fold in BA71V (Figure 4c).

202 This observation can at least in part be attributed to the larger number of viral genomes during late
203 infection, with increased levels of viral RNAP and associated factors available for transcription,
204 following viral protein synthesis. Viral DNA-binding proteins, such as histone-like A104R (51), may
205 remain associated with the genome originating from the virus particle in early infection. This could
206 suppress spurious transcription initiation, compared to freshly replicated nascent genomes that are

207 highly abundant in late infection. In order to test whether the increased mRNA levels correlated with
208 the increased number of viral genomes in the cell, we determined the viral genome copy number by
209 using quantitative PCR (qPCR against the p72 capsid gene sequence) using purified total DNA from
210 infected cells isolated at 0 hpi, 5 hpi and 16 hpi, and normalized values to the total amount of input
211 DNA. Using this approach, we observed genome copy levels that were consistent from 0 hpi to 5 hpi,
212 consistent with this being pre-DNA replication, followed by a substantial increase at 16 hpi, which was
213 more pronounced in BA71V infection (Figure 4d). This corresponded to a 15-fold increase in GRG
214 genome copy numbers from late, compared to early times post-infection of porcine macrophages,
215 and a 30-fold increase in BA71V during infection of Vero cells (Figure 4e). In summary, the ASFV
216 transcriptome changes both qualitatively and quantitatively as infection progresses, and the increase
217 of virus mRNAs during late infection is accompanied by the dramatic increase in viral genome copies.
218 Interestingly, the increase in viral transcripts and genome copies was less dramatic in the virulent GRG
219 strain.

220 [Correcting the bias of temporal expression pattern](#)

221 The standard methods of defining differential gene expression are well established in transcriptomics
222 using programs like DESeq2 (47). This is a very convenient and powerful tool which captures the
223 nuances of differential expression in complex organisms. However, virus transcription is often
224 characterised by more extreme changes, typically ranging from zero to millions of reads. Furthermore,
225 in both BA71V and GRG strains the genome-wide mRNA levels and total ASFV reads increase over the
226 infection time course (Figure 4 and Supplementary Table 1a). As a consequence, such normalisation
227 against the total mapped transcripts per sample (RPM) generates overestimated relative expression
228 values at 5 hpi, and understates those at 16 hpi (10). In order to validate the early-late expression
229 patterns derived from CAGE-seq, we carried out RT-PCR for selected viral genes, as this signal is
230 proportionate to the number of specific mRNAs regardless of the level of other transcripts – with the
231 minor caveat that it can pick up readthrough transcripts from upstream genes. We tested differentially
232 expressed conserved genes including GRG early- (MGF 505-7R, MGF 505-9R, NP419L), and D345L
233 which showed stable relative expression values (RPM values in Figure 1e). All selected genes showed
234 a consistently stronger RT-PCR signal during late infection in both BA71V and GRG (Figure 5a-d). The
235 exception is NP419L whose levels were largely unchanged, and this is an example of how a gene whose
236 transcript levels remain constant would be considered downregulated, when almost all other mRNA
237 levels increase (Figure 5b).

238 The standard normalisation of NGS reads against total mapped reads (RPM) is regularly used as it
239 enables a statistical comparison between samples and conditions, subject to experimental variations

240 (52). Keeping this in mind, we used an additional method of analysing the ‘raw’ read counts to
241 represent global ASFV transcript levels that are not skewed by the normalisation against total mapped
242 reads. Figure 5 shows a side-by-side comparison of RT-PCR results, and the CAGE-seq data normalised
243 (RPM) or expressed as raw counts, beneath each RT-PCR gel. Unlike CAGE-seq, RT-PCR will detect
244 transcripts originating from read-through of transcripts initiated from upstream TSS including intra-
245 ORF TSS (ioTSSs). To detect such ‘contamination’ we used multiple primer combinations in upstream
246 and downstream segments of the gene (Figure 5c, cyan and yellow arrows) to capture and account for
247 possible variations. Overall, our comparative analyses shows that the normalised data (RPM) of early
248 genes such as MGF 505-7R and 9R indeed skews and overemphasises their early expression, while the
249 raw counts are in better agreement with the mRNA levels detected by RT-PCR. In contrast, late genes
250 such as NP419L and D345L would be categorised as late using all three quantification methods, in
251 agreement with GRG CAGE-seq but not BA71V from Figure 3c. We validated the expression pattern of
252 the early GRG-specific gene MGF 360-12L (Figure 5e). While the RPM values indicated a very strong
253 decrease in mRNA levels from early to late time points, the decrease in raw counts was less
254 pronounced and more congruent with the RT-PCR analysis, showing a specific signal with nearly equal
255 intensity during early and late infection. Lastly, we used qRT-PCR to quantify C315R transcript levels,
256 as this was close to the early vs late threshold, (a log2fold change of 0 in Figure 3c), which showed
257 again that qRT-PCR better agreed with the raw counts.

258 An improved temporal classification of ASFV genes

259 Based on the considerations above, we prepared a revised classification of temporal gene expression
260 of the genes conserved between the two strains based on raw counts. The heatmap in Figure 6a shows
261 the mRNA levels at early and late infection stages of BA71V and GRG strains (all in duplicates) with the
262 genes clustered into five subcategories (1 to 5, Figure 6a) according to their early and late expression
263 pattern, which are shown in Figure 6b. Genes that are expressed at high or intermediate levels during
264 early infection but that also show high or intermediate mRNA levels during late infection are classified
265 as ‘early’ genes belonging to cluster-1 (8 genes, levels: high to high, H-H), cluster-4 (33 genes, mid to
266 mid, M-M) and cluster-5 (16 genes, low-mid to low-mid, LM-LM). Genes with low or undetectable
267 mRNA levels during early infection, which increase to intermediate or high levels during late infection
268 are classified as ‘late’ genes and belong to cluster-2 (15 genes, low to high, L-H) and cluster-3 (60
269 genes, low to mid, L-M), respectively. Overall, the clustered heatmap based on raw counts shows a
270 similar but more emphasised pattern compared to the normalised (RPM) data (compare Figure 6 and
271 Supplementary Figure 1). Calculating the percentage of reads per gene, which can be detected at 16
272 hpi compared to 5 hpi, reveals only a small number of genes have most ($\geq 70\%$) of their reads

273 originating during early infection: 30 genes in the GRG strain and 5 genes in the BA71V strain. For over
274 half of the BA71V-GRG conserved genes, 90-100 % of reads can be detected during late infection
275 (Figure 6c). For all GRG genes, this generates a significant difference between the raw counts per gene
276 between time-points (Figure 6d).

277 Below we discuss specific examples of genes subcategorised in specific clusters. I73R is among the top
278 twenty most-expressed genes during both early and late infection according to the normalised RPM
279 values (Figure 2c and d) resides in cluster-1 (H-H) (Figure 6a). While I73R is expressed during early
280 infection, the mRNA levels remain high with >1/3 of all reads detected during late infection in both
281 strains when calculated as raw counts (34 % in GRG and 45 % in BA71V). This new analysis firmly
282 locates I73R into cluster-1 (H-H) and is classified confidently as early gene. Notably, our new approach
283 results in biologically meaningful subcategories of genes that are likely to be coregulated, e. g. the
284 eight key genes that encode the ASFV transcription system including RNAP subunits RPB1 (NP1450L),
285 RPB2 (EP1242L), RPB3 (H359L), RPB5 (D205R), RPB7 (D339L) and RPB10 (CP80R), the transcription
286 initiation factor TBP (B263R) and the capping enzyme (NP868R) belong to cluster-4 (M-M), and
287 transcription factors TFIIS (I243L) and TFIIB (C315R) belong to cluster-5 (LM-LM). The overall mRNA
288 levels of cluster-4 and -5 genes are different, but remain largely unchanged during early and late
289 infection, consistent with the transcription machinery being required throughout infection. In
290 contrast, the mRNAs encoding the transcription initiation factors D6 (D1133L) and A7 (G1340L) are
291 only present at low levels during early- but increase during late infection and thus belong to cluster-3
292 (L-M), classifying them as late genes. This is meaningful since the heterodimeric D6-A7 factor is
293 packaged into viral particles (7), presumably during the late stage of the infection cycle. The mRNAs
294 of the major capsid protein p72 (B646L) and the histone-like-protein A104R (51,53) follow a similar
295 late pattern but are present at even higher levels during late infection and therefore belong to cluster-
296 2 (L-H).

297 Architecture of ASFV promoter motifs

298 In order to characterise early promoter motifs (EPM) in the GRG strain, we extracted sequences 35 bp
299 upstream of all early gene TSSs and carried out multiple sequence alignments. As expected, this region
300 shows a conserved sequence signature in good agreement with our bioinformatics analyses of EPMS
301 in the BA71V strain, including the correct distance between the EPM and the TSS (9-10 nt from the
302 EPM 3' end) and the 'TA' motif characteristic of the early gene Initiator (Inr) element (Figure 7a) (10).
303 A motif search using MEME (54) identified a core (c)EPM motif with the sequence 5'-AAAATTGAAT-3'
304 (Figure 7b), within the longer EPM. The cEPM is highly conserved and is present in almost all promoters
305 controlling genes belonging to cluster-1, -4 and -5 (Supplementary Table 3). A MEME analysis of
10

306 sequences 35 bp upstream of late genes (Figure 7c), provided a 17-bp AT-rich core late promoter motif
307 (cLPM, Figure 7d), however, this could only be detected in 46 of the late promoters.

308 In an attempt to improve the promoter motif analyses and deconvolute putative sequence elements
309 further, we probed the promoter sequence context of the five clusters (clusters 1-5 in Figure 7e-i,
310 respectively) of temporally expressed genes with MEME (Supplementary Table 3). The early gene
311 promoters of clusters-1 (H-H), -4 (M-M) and -5 (LM-LM) are each associated with different expression
312 levels, and all of them contain the cEPM located 15-16 nt upstream of the TSS with two exceptions
313 that are characterized by relatively low mRNA levels (Figure 7k). Interestingly, cluster-2 (L-H)
314 promoters are characterized by a conserved motif with significant similarity to eukaryotic TATA-box
315 promoter element that binds the TBP-containing TFIID transcription initiation factor (Figure 7f
316 highlighted with red bracket, detected via Tomtom (55) analysis of the MEME motif output). Cluster-
317 3 (L-M) promoters contain a long motif akin to the cLPM, derived from searching all late gene
318 promoter sequences, and which is similar to the LPM identified in BA71V (Figure 7d and g, green
319 bracket). All motifs described in the cluster analysis above could be detected with statistically
320 significance (p-value < 0.05) via MEME, in every gene in each respective cluster with only two
321 exceptions: MGF 110-3L from cluster-1, and MGF 360-19R from cluster-4, for the latter see details
322 below.

323 [Updating Genome Annotations using Transcriptomics Data](#)

324 TSS-annotation provides a useful tool for re-annotating predicted ORFs in genomes like ASFV (10)
325 where many of the gene products have not been fully characterized and usually rely on prediction
326 from genome sequence alone. We have provided the updated ORF map of the GRG genome in GFF
327 format (Supplementary Table 1f). This analysis identified an MGF 360-19R ortholog (Figure 8),
328 demonstrating how transcriptomics enhances automated annotation of ASFV genomes by predicting
329 ORFs from TSSs. The MGF 360-19R was included in subsequent DESeq2 analysis showing it was not
330 highly nor significantly differentially expressed (Supplementary Table 1e). Another important feature
331 is the identification of intra-ORF TSSs (ioTSSs) within MGF 360-19R that potentially direct the synthesis
332 of N-terminally truncated protein variants expressed either during early or late infection. The presence
333 of EPM and LPM promoter motifs lends further credence to the ioTSSs (Figure 8). Similar truncation
334 variants were previously reported for I243L and I226R (56) and in BA71V (10). In addition, we detected
335 multiple TSSs within MGF 360-19R encoding very short putative novel ORFs (nORF) 5, 7 or 12 aa
336 residues long; since these ioTSSs were present in both early and late infection they are not all likely to
337 be due to pervasive transcription during late infection.

338 We investigated the occurrence of iOTSS genome wide and uncovered many TSSs with ORFs
339 downstream that were not annotated in the GRG genome (Supplementary Table 2a). These ORFs
340 could be divided into sub-categories: in-frame truncation variants (Supplementary Table 2b, akin to
341 MGF 360-19R in Figure 8), nORFs (Supplementary Table 2c), and simply mis-annotated ORFs. All
342 updated annotations are found in Supplementary Table 1f. Putative truncation variants generated
343 from iOTSSs were predominantly identified during late infection, suggesting these could be a by-
344 product of pervasive transcription. Therefore, those detected early or throughout infection are
345 perhaps more interesting, they span a variety of protein functional groups, and many gene-products
346 are entirely uncharacterised (Figure 9a). The truncation variants additionally showed a size variation
347 of 5'-UTRs between the iOTSSs and downstream start codon (Figure 9b). An example of a mis-
348 annotation would be CP204L (Phosphoprotein p30, Figure 9c) gene that is predicted to be 201 residues
349 long. The TSS determined by CAGE-seq and validated by Rapid Amplification of cDNA Ends (5'-RACE)
350 is located downstream of the annotated start codon; based on our results we reannotated the start
351 codon of CP204L which results in a shorter ORF of 193 amino acids (Figure 9c).

352 Our GRG TSS map led to the discovery of many short nORFs, which are often overlooked in automated
353 ORF annotations due to a minimum size, e. g. 60 residues in the original BA71V annotation (15). Some
354 short ORFs have been predicted for the GRG genome including those labeled 'ASFV_G_ACD' in the
355 Georgia 2007/1 genome annotation (19). However, their expression was not initially supported by
356 experimental evidence, though we have now demonstrated their expression via CAGE-seq (Figure 2b,
357 Supplementary Table 1e). We have now identified TSSs for most of these short ORFs, indicating at
358 minimum they are transcribed. As described above, we noted that TSSs were found throughout the
359 genome in intergenic regions in addition to those identified upstream of the 190 annotated GRG ORFs
360 (including MGF 360-19R, Supplementary Table 2c). Our systematic, genome-wide approach identified
361 175 novel putative short ORFs. BLASTP (57) alignments showed that 13 were homologous to ORFs
362 predicted in other strains, including DP146L and pNG4 from BA71V . We validated the TSSs for these
363 candidates using 5'-RACE, which demonstrates the presence of these mRNAs and their associated TSSs
364 at both time-points (Figure 9d and e, respectively), compared to our CAGE-seq data (Figure 9f and g,
365 respectively).

366 Putative single-SH2 domain protein encoding genes in MGF 100

367 Our understanding of the ASFV genome is hampered by the large number of genes with unknown
368 functions. We approached this problem by searching for conserved domains of uncharacterised MGF
369 members *in silico*. MGF 100 genes form the smallest multigene family and include three short (100–
370 150 aa) paralogs located at both genome ends (right, R and left, L): 1R, 1L (MGF_100-2L or DP141L in
12

371 BA71V), and 3L (DP146L in BA71V). We predicted the two highly similar GRG ORFs I7L and I8L (51%
372 sequence identity) to belong to the MGF 100 family (Figure 10a), as designated in the Malawi LIL20/1
373 strain (58). Both I7L and I8L show similar overall transcript levels to the annotated MGF 100 members
374 -1L and 1R, though newly annotated MGF 100-3L (nORF_180573) was expressed at much higher levels.
375 I7L and I8L are both early genes like MGF 100-3L, while MGF 100-1L and 1R are expressed late and not
376 significantly changing, respectively (Supplementary Table 1e). Several lines of evidence suggest that
377 I7L and I8L play a role during infection. I7L and I8L are expressed early and at high levels, their
378 deletion along with L9R, L10L, and L11L ORFs reduces virulence in swine (59), and their loss is
379 associated with the adaptation of the GRG2007/1 strain to tissue culture infection (60). To gain insight
380 into the function of MGF family members including I7L and I8L, we generated computational
381 homology models of MGF 100-1L -1R, I7L and I8L using Phyre2 (61) (Figure 10b). The structures
382 selected by the algorithm for the modeling of MGF 100 proteins, included suppressor of cytokine
383 signalling proteins 1 and -2, and the PI3-kinase subunit alpha, all of which are characterized by Src
384 Homology 2 (SH2) domains (Figure 10b and Supplementary Table 2d). Canonical SH2 domains bind to
385 phosphorylated Tyrosine residues and are an integral part of signalling cascades involved in the
386 immune response (62). HHpred searches (63) predicted that indeed all MGF 100 members in BA71V
387 and GRG include SH2 domains (Figure 10c).

388 [The response of the porcine macrophage transcriptome to ASFV infection](#)

389 In order to evaluate the impact of ASFV on the gene expression of the host cell, we analysed
390 transcriptomic changes of infected porcine macrophages using the CAGE-seq data from the control
391 (uninfected cells), 5 hpi, and 16 hpi. We annotated 9,384 macrophage-expressed protein-coding genes
392 with CAGE-defined TSSs (Supplementary Table 4). Although primary macrophages are known to vary
393 largely in their transcription profile, the CAGE-seq reads were highly similar between RNA samples
394 obtained from macrophages from two different animals in this study (Spearman's correlation
395 coefficients ≥ 0.77).

396 As TSSs are not well annotated for the swine genome, we annotated them *de novo* using our CAGE-
397 seq data with the RECLU pipeline. 37,159 peaks could be identified, out of which around half (18,575)
398 matched unique CAGE-derived peaks annotated in Robert et al. (64) i.e. they were located closer than
399 100 nt to the previously described peaks. Mapping CAGE-seq peaks to annotated swine protein-coding
400 genes led to identification of TSSs for 9,384 macrophage-expressed protein-coding genes
401 (Supplementary Table 4). The remaining 11,904 swine protein-coding genes did not have assigned
402 TSSs, and therefore their expression levels were not assessed. The majority of genes were assigned
403 with multiple TSSs, and these TSS-assigned genes, corresponded to many critical functional
13

404 macrophage markers, including genes encoding 56 cytokines and chemokines (including CXCL2, PPBP,
405 CXCL8 and CXCL5 as the most highly expressed), ten S100 calcium binding proteins (S100A12, S100A8,
406 and S100A9 in the top expressed genes), as well as interferon and TNF receptors (IFNGR1, IFNGR2,
407 IFNAR1, IFNAR2, IFNLR1, TNFRSF10B, TNFRSF1B, TNFRSF1A, etc.), and typical M1/M2 marker genes
408 such as TNF, ARG1, CCL24, and NOS2 (Supplementary Table 5)

409 The 9,384 genes with annotated promoters were subjected to differential expression analysis using
410 DESeq2 to compare the 5 and 16 hour infected cell time points with control non-infected cells (c, 5
411 and 16) in a pairwise manner i.e. between each condition. Expression of only 25 host genes was
412 significantly deregulated between the control and 5 hpi, compared to 652 genes between 5 hpi and
413 16 hpi, and 1325 genes between mock-infected and 16 hpi (at FDR of 0.05). Based on the pairwise
414 comparisons, we could distinguish major response profiles of the host genes. Late response genes,
415 whose expression was significantly deregulated both between the uninfected control and 16 hpi and
416 5 and 16 hpi, and early response genes, whose expression was significantly deregulated between the
417 control and 5 hpi, but not 5-16 hpi (Figure 11a). The latter category included only 20 genes, whereas
418 more than 500 genes showed the late differentially regulated response: 344 genes were up-regulated,
419 and 180 genes were down-regulated. The majority of the > 9000 genes analysed therefore were not
420 differentially regulated. Comparison of differences between expression levels in the different samples
421 indicate that macrophage differentially expressed transcription programs change mostly between 5
422 and 16 hpi (Figure 11b and c). The upregulated late response genes with highest expression levels
423 included several S100 calcium binding proteins. In contrast, expression of important cytokines
424 (including CCL24, CXCL2, CXCL5 and CXCL8) significantly decreased from 5 hpi to 16 hpi (Figure 11d).

425 To investigate the transcriptional response pathways and shed light on possible transcription factors
426 involved in the macrophage response to ASFV infection, we searched for DNA motifs enriched in
427 promoters of the four categories of deregulated genes in Figure 11a. Both late response promoter sets
428 were significantly enriched with motifs, some of which contained sub-motifs known to be recognised
429 by human transcription factors (Supplementary Figure 2). The highest-scored motif found in
430 promoters of upregulated genes contained a sub-motif recognised by a family of human interferon
431 regulatory factors (IRF9, IRF8 and IRF8, (Supplementary Figure 2a) that play essential roles in the anti-
432 viral response. Interestingly, both upregulated and downregulated promoters (Supplementary Figure
433 2b and c, respectively) were enriched with extended RELA/p65 motifs. p65 is a Rel-like domain-
434 containing subunit of the NF-kappa-B complex, regulated by I-kappa-B, whose analog is encoded by
435 ASFV. This pathway being a known target for ASFV in controlling host transcription (65–68).

436 To understand functional changes in the macrophage transcriptome, we also performed gene set
437 enrichment analysis using annotations of human homologs. The top enriched functional annotations
438 in the upregulated late response genes include glycoproteins and disulfide bonds, transmembrane
439 proteins, innate immunity, as well as positive regulation of inflammatory response (Figure 11e). In
440 contrast, sterol metabolism, rRNA processing, cytokines, TNF signalling pathway, inflammatory
441 response as well as innate immunity were the top enriched functional clusters among the
442 downregulated late response genes. Interestingly, the genes associated with innate immunity appear
443 overrepresented in both up- and downregulated gene subsets, yet cytokines are 8-fold enriched only
444 in the downregulated genes). The mRNA levels of genes of interest were additionally verified using
445 RT-PCR (Figure 11f).

446 [Protein expression of selected genes.](#)

447 In order to determine whether the regulation exerted by GRG on host transcription of
448 immunomodulatory genes could also translate to protein levels, we selected representative proteins
449 whose genes showed significant changes. ISG15 expression, part of the antiviral response genes of the
450 type I IFN stimulation pathway, was measured with Western blot (Figure 12a), with ASFV infection
451 being monitored via P30 levels (Figure 12b). Cytokines released from infected PAMS were quantified
452 using ELISA tests for pig cytokines, TNF- α , CXCL8 and CCL2 (Figure 12c, d and e, respectively). As shown
453 in Figure 12, the release/expression for all the tested proteins during GRG infection were similar or
454 decreased in comparison to the control uninfected cells at both 5 hpi and 16 hpi, while the production
455 of viral protein P30 increased, confirming an effective viral infection.

456 [Discussion \[3,009 words\]](#)

457 In order to shed light on the gene expression determinants for ASF virulence, we focussed our analyses
458 on the similarities and differences in gene expression between a highly virulent Georgia 2007/1 isolate
459 and a nonvirulent, lab-adapted strain BA71V. Previous annotation identified 125 ASFV ORFs that are
460 conserved between all ASFV strain genomes irrespective of their virulence (16). They represent a 'core'
461 set of genes required for the virus to produce infectious progeny and include gene products like those
462 involved in virus genome replication, virion assembly, RNA transcription and modification. These
463 genes are located in the central region of the genome (Figure 1a). Besides such essential genes, about
464 one third are non-essential for replication, but have roles in evading host defence pathways. Some
465 genes are conserved between isolates, but not necessarily essential core genes, for example apoptosis
466 inhibitors: Bcl-2 family member A179L and IAP family member A224L (69). Other non-essential genes,
467 especially MGF members, vary in number between isolates. Our transcriptomic analysis captured TSS

468 signals from 119 genes both shared between the BA71V and GRG genomes, which also matched
469 expression patterns during early and late infection, according to CAGE-seq (Figure 3, Figure 4a-c).
470 Outliers include DP148R, which is unsurprising, given its promoter region is deleted in BA71V, and its
471 coding region is interrupted by a frame shift mutation, therefore functional protein expression
472 unlikely. DP148R is a non-essential, early-expressed virulence factor in the Benin 97/1 strain (49) –
473 consistent with our GRG data. Many additional GRG genes, lost from BA71V are MGFs, which are
474 mostly upregulated during early infection and located at the ends of the linear genome (Figure 1a).
475 MGFs have evolved on the virus genome by gene duplication, and do not share significant similarity
476 to other proteins, though some conserved domains, including ankyrin repeats, are present in some
477 MGF 360 and 505 family members (17,19).

478 Using advanced sequence searches and computational homology modelling we predict the members
479 of the MGF 100 family to encode SH2 domains, including I7L and I8L. Although SH2 domains are
480 primarily specific to eukaryotes, rare cases of horizontally transferred SH2 domains found in viruses,
481 are implicated in hijacking host cell pTyr signalling (70). A large family of ‘super-binding’ SH2 domains
482 were discovered in *Legionella*. Its members, including single SH2 domain-proteins are likely effector
483 proteins during infection (71). We also identified a further MGF 100 member in the GRG genome as
484 one of our nORFs, a partial 100-residue copy of DP146L (MGF 100-3L) (Supplementary Table 2c).
485 Unlike its annotated MGF 100-1L and MGF 100-1R cousins it was downregulated from 5 hpi to 16 hpi
486 (Supplementary Table 1e). Together with I7L and I8L, GRG encodes a total of 5 MGF 100 genes (Figure
487 10a). Interestingly, loss of MGF 100 members was observed during the process of adapting a virulent
488 Georgia strain to grow in cultured cell lines (60). Deletion of MGF 100-1R, from a virulent genotype II
489 Chinese strain (72) or of I8L from Georgia 2010 was shown not to reduce virulence of the virus in pigs
490 or reduce virus replication in porcine macrophages (73). However, simultaneous deletion of genes I7L,
491 I8L, I9L, I10L and I11L from a Chinese virulent isolate reduced virulence and surviving pigs were
492 protected against challenge (59). In summary, although deletion of some individual MGF 100 genes
493 does not lead to attenuation, deletion of I7L and I8L, in combination with I9L, I10L, and I11L did have
494 an impact.

495 The Georgia 2007/1 genome was recently re-sequenced which identified a small number of genome
496 changes affecting mapped ORFs and identified new ORFs (18). Adjacent to the covalently cross-linked
497 genome termini, the BA71V genome contains terminal inverted repeats of >2 kbp, in which two short
498 ORFs were identified (DP93R, DP86L). These were not included in previous GRG sequence annotations,
499 however our nORFs included a 55-residue homolog of DP96R, which was a late, but not highly
500 expressed gene. These are yet further examples of how transcriptomics aid in improving ASFV genome

501 annotation. Functional data is available for only a few of proteins coded by ORFs not conserved
502 between BA71V and GRG. This includes the p22 protein (KP177R), which is expressed on the cell
503 membrane during early infection, and also incorporated into the virus particle inner envelope. The
504 function of the KP177R-like GRG gene l10L has not been studied, but may provide an antigenically
505 divergent variant of P22, enabling evasion of the host immune response (19). We found KP177R was
506 highly expressed at 16 hpi, while l10L was also expressed late, but at much lower levels. Their function
507 is unknown, though the presence of an SH2 domain indicates possible roles in signalling pathways
508 (7,19,74).

509 MGF 110 members are among the highest expressed genes during early infection both in GRG (this
510 study), and in BA71V (10), suggesting high importance during infection, at least in porcine
511 macrophages and Vero cells, respectively. However, MGF 110 remains poorly characterised, and 13
512 orthologues were identified thus far, with numbers present varying between isolates (30). MGF 110
513 proteins possess cysteine-rich motifs, optimal for an oxidizing environment as found in the
514 endoplasmic reticulum (ER) lumen or outside the cell, and MGF 110-4L (XP124L) contains a KDEL signal
515 for retaining the protein in the ER (75). Since highly virulent isolates have few copies of these genes
516 (for example, only 5 in the Benin 97/1 genome), it was assumed they are not importance for virulence
517 in pigs (17), but their high expression warrant further investigation, which has recently begun in the
518 form of deletion mutants. For example, deletion of MGF 110-9L from a Chinese genotype II virulent
519 strain, reduced virulence (35), whereas deletion of MGF 110-1L from Georgia 2010 (76) did not
520 substantially affect virulence.

521 There is however, good evidence that MGF 360 and 505 carry out important roles in evading the host
522 type I interferon (IFN) response - the main host antiviral defence pathway (37). Evidence for the role
523 of MGF 360 and 505 genes in virulence was obtained from deletions in tissue-culture adapted and
524 field attenuated isolates, as well as targeted gene deletions This correlated with induction of the type
525 I interferon response, which itself is inhibited in macrophages infected with virulent ASFV isolates
526 (32,38,39). Deletions of these MGF 360, and 505 genes also correlated with an increased sensitivity of
527 ASFV replication, to pre-treatment of the macrophage cells with type I IFN (40). Thus, the MGF 360
528 and 505 genes have roles in inhibiting type I IFN induction and increasing sensitivity to type I IFN.
529 However, it remains unknown if these MGF 360 and MGF 505 genes act synergistically or if some have
530 a more important role than others type I IFN suppression. Our DESeq2 analysis did show that members
531 of both these families showed very similar patterns of early expression (Figure 2 and Figure 3),
532 conserved cEPM-containing promoters, and almost exclusive presence in clusters-1 (H-H), -4 (M-M),

533 and -5 (LM-LM) (Figure 6 and Figure 7), consistent with ASFV prioritising inhibition of the host immune
534 response during early infection.

535 An interesting pattern which emerged during our CAGE-seq analysis was the clear prevalence of ioTSSs
536 within ORFs, especially in MGFs (Figure 8 and Figure 9). However, it is not clear whether subsequent
537 in-frame truncation variants generate stable proteins, nor what their function could be. Perhaps even
538 more interesting was the discovery of 176 nORFs (including MGF 360-19R), with clear TSSs according
539 to CAGE-seq, highlighting the power of transcriptomics to better annotate sequenced genomes. We
540 were able to detect previously unannotated genes from other strains, and partial duplications of genes
541 already encoded in GRG (Supplementary Table 2).

542 The increase in transcription across the ASFV genome during late infection (10), appears ubiquitous.
543 At least 50 genes have previously been investigated in single gene expression studies using Northern
544 blot or primer extension (for review see references (10,77). Transcripts from over two thirds of these
545 genes were detected during late infection, and a quarter had transcripts detected during both early
546 and late infection. Therefore, clear evidence using several techniques now support this increase in
547 ASFV transcripts at late times post-infection. It is not entirely clear whether it is due to pervasive
548 transcription, high mRNA stability or a combination of factors. However, there is a correlated increase
549 in viral genome copies, potentially available as templates for pervasive transcription. The increase in
550 genome copies is more pronounced in BA71V compared to GRG, which likewise is reflected in the
551 increase in transcripts during late infection (Figure 4).

552 Our transcriptomic analysis of the porcine macrophage host revealed 522 genes whose expression
553 patterns significantly changed between 5 and 16 hrs post-infection (Figure 11a) and only 20 genes
554 were found to change between the control cells and those infected for 5 hpi. In aggregate, this reflects
555 a relatively slow host response to ASFV infection following expression of early ASFV genes. We
556 observed mild downregulation of some genes e.g. ACTB coding for β -actin, eIF4A, and eIF4E
557 (Supplementary Table 5), resembling patterns previously shown by RT-qPCR (78). The macrophage
558 transcriptome mainly shuts down immunomodulation between 5 hpi to 16 hpi post-infection;
559 cytokines appeared highly expressed at 5 hpi, but downregulated from 5 hpi to 16 hpi. Of the 54
560 cytokine genes we detected, expression of thirteen was decreased: four interleukin genes (IL1A, IL1B,
561 IL19, IL27), four pro-inflammatory chemokines (CCL24, CXCL2, CXCL5, CXCL8), and tumor necrosis
562 factor (TNF) genes. Since inflammatory responses serve as the first line of host defense against viral
563 infections, viruses have developed ways to neutralise host pro-inflammatory pathways. ASFV encodes
564 a structural analog of I κ B, A238L, which was proposed to act as a molecular off-switch for NF κ B-

565 targeted pro-inflammatory cytokines (67). In our study, A238L is one of the most expressed ASFV
566 genes at 5 hpi, but significantly downregulated afterwards (Figure 2c). Accordingly, swine homologs
567 of human NF κ B target genes were significantly over-represented (3.8 fold) among downregulated
568 macrophage genes (Fisher's exact p-value < 1e-5, based on human NF κ B target genes from
569 <https://www.bu.edu/nf-kb/gene-resources/target-genes/>). Downregulated genes include
570 interleukins 1A, 1B, and 8, and 27 (IL1A, IL1B, CXCL8, IL27), TNF, as well as a target for common
571 nonsteroidal anti-inflammatory drugs, prostaglandin-endoperoxide synthase 2 (PTGS2 or COX-2)
572 (Supplementary Figure 2). Interestingly, promoters of both up- and downregulated genes contained a
573 motif with the sequence preferentially recognised by the human p65-NF κ B complex (79). Expression
574 of TNF, a well-known marker gene for acute immune reaction and M1 polarisation, was recorded at a
575 high level in control samples and at 5 hpi, but significantly dropped at 16 hpi. It has been already
576 shown that ASFV inhibits transcription of TNF and other proinflammatory cytokines (67). On the other
577 hand, the downregulation of TNF stands in contrast to previous results from ASFV-E75 strain-infected
578 macrophages in vitro, where TNF expression increased significantly after 6 hpi (80). Therefore, the
579 different time courses of TNF expression induced by the moderately virulent E75 and more virulent
580 Georgia strain may reflect different macrophage activation programs (81).

581 We investigated if the modulation of transcription we observed by CAGE-seq during GRG infection of
582 PAMS was also observed at the protein level. We analysed the secretion or expression of different
583 immunomediators (cytokines CCL2, CXCL8, TNF- α and interferon stimulated gene ISG15) at different
584 times following infection of PAMS. We confirmed that that the infection did not lead to an increase of
585 these mediators at either 5h or 16h infection. Secretion or expression of these proteins were similar
586 or slightly decreased in infected cells in comparison to control non-infected cells. The results indicated
587 that the control by virulent Georgia 2007/1 of host cell responses to infection we observed at the
588 transcription level can lead to a control also at the level of the protein production. Interestingly, CCL2
589 transcription was somewhat upregulated at late infection (Supplementary Table 5), whereas its
590 protein release to the supernatant was decreased (Figure 12e). ASFV has been shown to prioritize
591 expression of its encoded proteins by sequestering components of the host translation machinery to
592 viral factories (82). The levels or functions of host proteins may also be modulated by targeting for
593 post-translational modification or degradation (82–84). Therefore, in addition to control at the
594 transcriptional level ASFV may modulate the production of immunomodulatory host proteins at a later
595 step, as seems to occur for CCL2, a known chemoattractant for myeloid and lymphoid cells (85), that
596 could be an important target for regulation by ASFV.

597 Four S100 family members are among the host genes that are upregulated after 5 hpi (Figure 11b)
598 including S100A8, S100A11, S100A12, and S100A13. S100A8 and S100A12 are among the most highly
599 expressed genes on average throughout infection. S100 proteins are calcium-binding cytosolic
600 proteins that are released and serve as a danger signal, and stimulate inflammation (86). Once
601 released from the cell, S100A12 and S100A8 function as endogenous agonists to bind TLR4 and induce
602 apoptosis and autophagy in various cell types (86). S100A8 and S100A9 were also found in the RNA-
603 seq whole blood study as the top upregulated upon infection of the pigs with Georgia 2007/1, but not
604 of a low pathogenic ASFV isolate OURT 88/3 (43).

605 Previous studies described global swine transcriptome changes upon ASFV infection using short read
606 sequencing (Illumina): including the RNA-seq described above (43) and a microarray study of primary
607 swine macrophage cell cultures infected with the GRG strain, at six time points post-infection (42).
608 Although these varied in designs and selected methods, results of these works both give some
609 indication into the main host immune responses and ways how ASFV could evade them. The latter
610 microarray study indicated similar suppression of inflammatory response after 16 hpi as we observed
611 in this study, with expression of many cytokines down-regulated relative to non-infected macrophages
612 (42). More-recently, there have been several transcriptomic studies using classical RNA-seq of ASFV
613 infections from Chinese isolates (44–46). Fan et al (44) investigated the transcriptomic and proteomic
614 response within tissues of pigs following ASFV infection and death, though this was not directly
615 comparable to our own analysis in PAMs, due to their observations being of a far later infection stage
616 (post-mortem) than our 16 hrs time-point. The two most-comparable studies to ours were carried out
617 on a Chinese genotype II pathogenic strain during infection of PAMs. Ju et al. (45) investigated 6, 12
618 and 24 hpi, while Yang et al. (46) investigated 12, 24, and 36 hpi. However, comparison of the
619 overlapping time points of 12 hpi and 24 hpi did not yield similar host gene expression changes,
620 possibly due to variation among primary macrophages or due to the low MOI of 1 used in both studies.
621 In summary, these differences highlight that our understanding of the host-virus relationship during
622 ASFV infection is still not well understood, and further work is needed to understand why such
623 substantial variation in host gene expression can arise.

624 A further important note, is that all of the studies described above are using classical RNA-seq-based
625 methods, the nucleotide resolution of which, is not sufficient to investigate differential expression of
626 both the virus and host simultaneously. Investigating the viral transcriptome is especially difficult in a
627 compact genome like that of ASFV, where transcription read-through can undermine results from
628 classical RNA-sequencing techniques (10,87). A recent investigation into ASFV RNA transcripts using
629 long-read based Oxford Nanopore Technologies (ONT) – provides fascinating insight into their length

630 and read-through heterogeneity. This new method highlighted how misleading short read sequencing
631 with classical RNA-seq can be when quantifying ASFV gene expression, due to the abundance of
632 readthrough occurring in ASFV, generating transcripts covering multiple viral ORFs. This study did
633 however, unfortunately lack the read coverage for in-depth analysis of host transcripts alongside that
634 of viral transcripts (88,89).

635 Here we have demonstrated that CAGE-seq is an exceptionally powerful tool for quantifying relative
636 expression of viral genes across the ASFV genome, as well as making direct comparison between
637 strains for expression of shared genes, and further highlighting the importance of highly-expressed
638 but still functionally uncharacterised viral genes. CAGE-seq conveniently circumvents the issue in
639 compact viral genomes like those of ASFV and VACV, of transcripts reading through into downstream
640 genes which cannot be distinguished from classical short-read RNA-seq (10,43,90). Furthermore, it
641 enables us to effectively annotate genome-wide, the 5' ends of capped viral transcripts, and thus TSSs
642 of viral genes, and subsequently their temporal promoters. This 5' end resolution in ASFV is still not
643 achievable via ONT long read sequencing (88,89). We have now expanded on promoter motifs we
644 previously described (Figure 7), to identify 5 clusters of genes (Figure 6), with distinct patterns of
645 expression. Three of these clusters (-1: high to high levels, -4: mid to mid, and -5 low-mid to low-mid)
646 have slightly differing promoters, with a highly conserved core EPM. This is akin to the early gene
647 promoter of VACV (87) for VETF recognition and early gene transcription initiation (13,91,92). We have
648 found late genes can be categorised into two types that either increase from low to extremely high
649 expression levels (e. g. p72-encoding B646L) in cluster-2, or from low to medium expression levels in
650 cluster 3 (e. g. VETF-encoding genes). The promoters of these genes show resemblance to the
651 eukaryotic TATA-box (93) or the BA71V LPM (10), respectively. Our analysis additionally shows the
652 potential for a variety of non-pTSSs: alternative ones used for different times in infection, ioTSSs which
653 could generate in-frame truncation variants of ORFs, sense or antisense transcripts relative to
654 annotated ORFs, and finally TSSs generating nORFs, which predominantly have no known homologs.

655 In summary, it is becoming increasingly clear that the transcriptomic landscape of ASFV and its host
656 during infection is far more complex than originally anticipated. Much of this raises further questions
657 about the basal mechanisms underlying ASFV transcription and how it is regulated over the infection
658 time course. Which subsets of initiation factors enable the RNAPs to recognise early and late
659 promoters? Does ASFV include intermediate genes, and what factors enables their expression? What
660 is the molecular basis of the pervasive transcription during late infection? The field of ASFV
661 transcription has been understudied and underappreciated and considering the severe threat that ASF
662 poses for the global food system and -food security, we now need to step up and focus our attention

663 and resources to study the fundamental biology of ASFV to develop effective antiviral drugs and
664 vaccines.

665 Methodology [2871 words]

666 GRG-Infection of Macrophages and RNA-extraction

667 Primary porcine alveolar macrophage cells were collected from two animals following approval by the
668 local Animal Welfare and Ethical Review Board at The Pirbright Institute. Cells were seeded in 6-well
669 plates (2×10^6 cells/well) with RPMI medium (with GlutaMAX), supplemented with 10% Pig serum and
670 100 IU/ml penicillin, 100 μ g/ml streptomycin. They were infected as 2 replicate wells for 5 hpi or 16
671 hpi with a multiplicity of infection (MOI) of 5 of the ASFV Georgia 2007/1 strain, while uninfected cells
672 were seeded in parallel as a control (mock-infection). Total RNA was extracted according to
673 manufacturer's instructions for extraction with Trizol Lysis Reagent (Thermo Fisher Scientific and the
674 subsequent RNAs were resuspended in 50 μ l RNase-free water and DNase-treated (Turbo DNase-free kit,
675 Invitrogen). RNA quality was assessed via Bioanalyzer (Agilent 2100). 5 μ g of each sample was ethanol
676 precipitated before sending to CAGE-seq (Kabushiki Kaisha DNAFORM, Japan). Samples were named
677 as follows: uninfected cells or 'mock' (C1-ctrl and C2-ctrl), at 5 hpi post-infection (samples G1-5h and
678 G2-5h), and at 16 hpi post-infection (G3-16h and G4-16h).

679 CAGE-sequencing and Mapping to GRG and *Sus scrofa* Genomes

680 Library preparation and CAGE-sequencing of RNA samples was carried out by CAGE-seq (Kabushiki
681 Kaisha DNAFORM, Japan). Library preparation produced single-end indexed cDNA libraries for
682 sequencing: in brief, this included reverse transcription with random primers, oxidation and
683 biotinylation of 5' mRNA cap, followed by RNase ONE treatment removing RNA not protected in a
684 cDNA-RNA hybrid. Two rounds of cap-trapping using Streptavidin beads, washed away uncapped RNA-
685 cDNA hybrids. Next, RNase ONE and RNase H treatment degraded any remaining RNA, and cDNA
686 strands were subsequently released from the Streptavidin beads and quality assessed via Bioanalyzer.
687 Single strand index linker and 3' linker was ligated to released cDNA strands, and primer containing
688 Illumina Sequencer Priming site was used for second strand synthesis. Samples were sequenced using
689 the Illumina NextSeq 500 platform producing 76 bp reads. FastQC (94) analysis was carried out on all
690 FASTQ files at Kabushiki Kaisha DNAFORM and CAGE-seq reads showed consistent read quality across
691 their read-length, therefore, were mapped in their entirety to the GRG genome (FR682468.1) in our
692 work using Bowtie2 (95), and *Sus scrofa* (GCF_000003025.6) genome with HISAT2 (95,96) by Kabushiki
693 Kaisha DNAFORM.

694 Transcription Start Site-mapping Across Viral GRG Genome

695 CAGE-seq mapped sample BAM files were converted to BigWig (BW) format with BEDtools (97)
696 genomecov, to produce per-strand BW files of 5' read ends. Stranded BW files were input for TSS-
697 prediction in RStudio (98) with Bioconductor (99) package CAGEfightR (100). Genomic feature
698 locations were imported as a TxDb object from FR682468.1 genome gene feature file (GFF3).
699 CAGEfightR was used to quantify the CAGE reads mapping at base pair resolution to the GRG genome
700 - at CAGE TSSs, separately for the 5 hpi and 16 hpi replicates. TSS values were normalized by tags-per-
701 million for each sample, pooled, and only TSSs supported by presence in both replicates were kept.
702 TSSs were assigned to clusters, if within 25 bp of one another, filtering out pooled, RPM-normalized
703 TSS counts below 25 bp for 5 hpi samples, or 50 bp for 16 hpi, and assigned a 'thick' value as the
704 highest TSS peak within that cluster. A higher cut-off for 16 hpi was used to minimise the extra noise
705 of pervasive transcription observed during late infection (10). TSS clusters were assigned to annotated
706 FR682468.1 ORFs using BEDtools intersect, if its highest point ('thick' region) was located within 500
707 bp upstream of an ORF, 'CDS' if within the ORF, 'NA' if no annotated ORF was within these regions.
708 Multiple TSSs located within 500 bp of ORFs were split into subsets: 'Primary' cluster subset contained
709 either the highest scoring CAGEfightR cluster or the highest scoring manually-annotated peak (when
710 manual ORF corrections necessary), and the highest peak coordinate was defined as the primary TSS
711 (pTSS) for an ORF. Further clusters associated with these ORFs were classified as 'non-primary', with
712 their highest peak as a non-primary TSS (npTSS). If the strongest TSS location was intra-ORF, without
713 any TSSs located upstream of the ORF, then the ORF was manually re-defined as starting from the next
714 ATG downstream.

715 DESeq2 Differential Expression Analysis of GRG Genes

716 For analysing differential expression with the CAGE-seq dataset, a GFF was created with BEDtools
717 extending from the pTSS coordinate, 25 bp upstream and 75 bp downstream, however, in cases of
718 alternating pTSSs this region was defined as 25 bp upstream of the most upstream pTSS and 75 bp
719 downstream of the most downstream pTSS. HTSeq-count (101) was used to count reads mapping to
720 genomic regions described above for both the RNA- and CAGE-seq sample datasets. The raw read
721 counts were then used to analyse differential expression across these regions between the time-
722 points using DESeq2 (default normalisation described by Love et al. (47)) and those regions showing
723 changes with an adjusted p-value (padj) of <0.05 were considered significant. A caveat of this 'early'
724 or 'late' definition is that it is a binary definition of whether a gene is up- or downregulated between
725 conditions (time-points), relative to the background read depth of reads, which map to the genome

726 in question. Further analysis of ASFV genes used their characterised or predicted functions, from the
727 VOCS tool database (<https://4virology.net/>) (102,103) entries for the GRG genome.

728 Quantification of viral genome copies at different time points of infection

729 Porcine lung macrophages were seeded and infected as described above. *Vero* cells were similarly
730 cultured in 6-well plates in DMEM medium supplemented with 10% Fetal calf serum, 100 IU/ml
731 penicillin and 100 µg/ml streptomycin, when semi-confluent they were infected with MOI 5 of Ba71V.
732 Immediately after infection (after 1h adsorption period, considered '0 hpi), or at 5 hpi, and 16 hpi, the
733 supernatant was removed and nucleic acids were extracted using the Qiamp viral RNA kit (Qiagen)
734 and quantified using a NanoDrop spectrophotometer (ThermoFisher Scientific). For quantification of
735 viral genome copy equivalents, 50 ng of each nucleic acid sample was used in qPCR with primers and
736 probe targeting the viral capsid gene B646L. As previously described (104), standard curve
737 quantification qPCR was carried out on a Mx3005P system (Agilent Technologies) using the primers
738 CTGCTCATGGTATCAATCTTATCGA and GATACCACAAGATC(AG)GCCGT and probe 5'-(6-
739 carboxyfluorescein [FAM])-CCACGGGAGGAATACCAACCCAGTG-3'-(6-carboxytetramethylrhodamine
740 [TAMRA]).

741 Analysis of mRNA levels by RT-PCR and quantitative real time PCR (qPCR)

742 RNA from GRG or Ba71V infected macrophages, or *Vero* cells respectively, or from uninfected cell
743 controls, was collected at the different time points post-infection with Trizol, as described above. RNA
744 was reverse transcribed (800 ng RNA per sample) using SuperScript III First-Strand Synthesis System
745 for RT-PCR and random hexamers (Invitrogen). For PCR, cDNAs were diluted 1:20 with nuclease free
746 water and 1 µl each sample was amplified in a total volume of 20 µl using Platinum™ Green Hot Start
747 PCR Master Mix (Invitrogen) and 200 nM of each primer. Annealing temperatures were tested for each
748 primer pair in gradient PCR to determine the one optimal for amplification.

749 Supplementary Table 7a shows the primers used for each gene target, the amplicon size, PCR reaction
750 conditions, and NCBI accession numbers for sequences used primer design. PCRs were then
751 performed with limited cycles of amplification to have a semi-quantitative comparison of transcript
752 abundance between infection timepoints (by not reaching the maximum product amplification
753 plateau). Amplification products were viewed using 1.5% agarose gel electrophoresis.

754 C315R transcript levels were assessed by qPCR, using housekeeping gene glyceraldehyde-3-phosphate
755 dehydrogenase (GAPDH) expression was used for normalisation. Primer details and the qPCR
756 amplification program are shown in

757 Supplementary Table 7b (GAPDH primers used for *Vero* cells were previously published by
758 Melchjorsen et al., 2009 (105)). Primers were used at 250 nM concentration with Brilliant III Ultra-Fast
759 SYBR® Green QPCR Master Mix (Agilent 600882), 1 µl cDNA in 20 µl (1:20) total reaction volumes, and
760 qPCRs carried out in Mx3005P system (Agilent Technologies). Similar amplification efficiencies (97-
761 102%) for all primers had been observed upon amplification of serially diluted cDNA samples, and the
762 relative expression at each timepoint of infection was calculated using the formula $2^{\Delta Ct}$ ($2^{Ct_{GAPDH} - Ct_{C315R}}$).
763

764 Preparation of supernatant and cell lysis extracts for ELISA and Western blot detection 765 of host proteins

766 Lung macrophage cultures from two donor outbred pigs (same cells used for CAGEseq) were prepared
767 in 6-well plates. Approximately 1.5×10^6 cells were seeded per well with 3 ml medium (RPMI with
768 penicillin/streptomycin and 10% pig serum) and incubated at 37 degrees 5% CO₂ overnight. Cultures
769 were washed once with culture medium to remove non-adherent cells and inoculated with MOI 5 of
770 ASFV-Georgia 2007/1 (or left uninfected as control) and centrifuged 1h at 600xg 26 degrees
771 (adsorption period). Supernatants from cell cultures were collected immediately after adsorption for
772 obtaining the 0 hpi timepoint and stored at -70 degrees until analysis. Adherent cells were washed
773 twice with cold DPBS (Sigma) and then lysed with 0.12 ml/well cold RIPA buffer (Thermo Scientific)
774 supplemented with protease inhibitors (Halt Protease Inhibitor Cocktail, Thermo Scientific). For 5h
775 and 16h timepoints, the inoculum was removed after adsorption, cells were washed twice in culture
776 medium and returned to the incubator with fresh 3 ml medium per well for the specified times of
777 infection. Supernatants and lysis volumes were collected similarly to the control. Supernatants were
778 analysed for the presence of CCL2 (Porcine CCL2/MCP-1 ELISA Kit, ES2RB Invitrogen), CXCL8
779 (Quantikine® ELISA, Porcine IL-8/CXCL8 Immunoassay, P8000 R&D) and TNF-α (Quantikine® ELISA,
780 Porcine TNF-α Immunoassay, PTA00 R&D) as recommended by the manufacturers. A volume of 25 µl
781 each lysate was analysed in Western Blot for expression of ISG15 (anti-ISG15 antibody ab233071,
782 Abcam; used at 1:1000 dilution), γ-Tubulin (anti-gamma Tubulin antibody ab11321, Abcam; used at
783 1:1000 dilution); and viral ASFV protein P30 (in-house mouse monoclonal antibody used at 1:500
784 dilution). Secondary antibodies used were Goat Anti-Rabbit IgG H&L (HRP) (ab205718, Abcam) and
785 Goat Anti-Mouse Immunoglobulins/HRP (P0447, Dako) both at 1:2000 dilution. Western blot
786 membranes were revealed using Pierce ECL Western Blotting Substrate (32106, Thermo Scientific).
787 Band densities were quantified using ImageJ (Rasband, W.S., ImageJ, U. S. National Institutes of
788 Health, Bethesda, Maryland, USA, <https://imagej.nih.gov/ij/>, 1997-2018).

789 ASFV Promoter Motif Analysis

790 DESeq2 results were used to categorise ASFV genes into two simple sub-classes: early; 87 genes
791 downregulated from early to late infection and late; the 78 upregulated from early to late infection.
792 These characterised gene pTSSs were then pooled with the nORF pTSSs, and sequences upstream and
793 downstream of the pTSS were extracted from the GRG genome in FASTA format using BEDtools.
794 Sequences 35 bp upstream of and including the pTSSs were analysed using MEME software
795 (<http://meme-suite.org>) (106), searching for 5 motifs with a maximum width of 20 nt and 27 nt,
796 respectively (other settings at default). The input for MEME motif searches included sequences
797 upstream of 134 early pTSSs (87 genes and 47 nORFs) for early promoter searching, while 234 late
798 pTSSs (78 genes and 156 nORFs) were used to search for late promoters. For analysis of conserved
799 motifs upstream of the five clusters described in Figure 6a-b, sequences were extracted in the same
800 manner as above, but grouped according to their cluster. MEME motif searches were carried out for
801 sequences in each cluster, searching for 3 motifs, 5-36 bp in length, with zero or one occurrence per
802 sequence ('zoops' mode).

803 Identification of TSSs by rapid amplification of cDNA ends - 5'RACE

804 For 5'RACE of GRG genes DP146L, pNG4 and CP204L we designed the gene specific primers (GSP)
805 shown in

806 Supplementary Table 7c, and used the kit: "5' RACE System for Rapid Amplification of cDNA Ends"
807 (Invitrogen), according to manufacturer instructions. Briefly, 150 ng RNA from either 5 hpi or 16 hpi
808 macrophages (one of the replicate RNA samples used for CAGE-seq) was used for cDNA synthesis with
809 GSP1 primers, followed by degradation of the mRNA template with RNase Mix, and column
810 purification of the cDNA. A homopolymeric tail was added to the cDNA 3'ends with Terminal
811 deoxynucleotidyl transferase, which allowed PCR amplification with an "Abridged Anchor Primer"
812 (AAP) from the 5'RACE kit and a nested GSP2 primer. A second PCR was performed over an aliquot of
813 the previous, with 5'RACE "Abridged Universal amplification Primer" (AUAP), and an additional nested
814 primer GSP3, except for pNG4 where GSP2 was re-used due to the small predicted size of the
815 amplicon. Platinum™ Green Hot Start PCR Master Mix (Invitrogen) was used for PCR and products
816 were run in 2% agarose gel electrophoresis (see

817 Supplementary Table 7c for expected sizes). Efficient recovery of cDNA from the purification column
818 requires a product of at least 200 bases and therefore, due to the small predicted size of pNG4
819 transcripts its GSP1 primer was extended at the 5' end with an irrelevant non-annealing sequence of
820 extra 50 nt in order to create a longer recoverable product.

821 CAGE-seq Analysis for the *Sus scrofa* Genome

822 Analyses of TSS-mapping, gene expression and motif searching with CAGE-seq reads mapped to the
823 *Sus scrofa* 11.1 genome were carried out by DNAFORM (Yokohama, Kanagawa, Japan). The 5' ends of
824 CAGE-seq reads were utilised as input for the Reclu pipeline (107) with a cutoff of 0.1 RPM, and
825 irreproducible discovery rate of 0.1. 37,159 total CAGE-seq peaks could be identified, of which around
826 half (16,720) match unique CAGE peaks previously identified by Roberts et al. (64) (i.e. within 100 nt
827 of any of them). TSSs for 9,384 protein-coding genes (out of 21,288) were annotated de novo from
828 the CAGE-defined TSSs (Supplementary Table 4).

829 Protein-coding genes with annotated TSSs (9,384 out of 21,288) were then subjected to differential
830 expression analysis. CAGE-seq reads were summed up over all TSSs assigned to a gene and compared
831 between two time points using edgeR (108) at maximum false discovery rate of 0.05. The full list of
832 host genes with annotated promoters together with their estimated expression levels is provided in
833 Supplementary Table 5. Gene set enrichment analysis was performed with the DAVID 6.8
834 Bioinformatics Resources (109), using best BLASTP (110) human hits (from the UniProt (111) reference
835 human proteome). The 9,331 genes with human homologs were used as a background, and functional
836 annotations of the four major expression response groups (late/early up-/down-regulated genes)
837 were clustered in DAVID 6.8 using medium classification stringency. MEME motif searches were
838 conducted for promoters of four differentially regulated subsets of host genes, as defined in Figure
839 11a. Promoters sequences were extended 1000 bp upstream and 200 bp downstream of TSSs,
840 searched with MEME (max. 10 motifs, max. 100 bp long, on a given strand only, zero or one site per
841 sequence, $E < 0.01$), and then compared against known vertebrate DNA motifs with Tomtom (p -value
842 < 0.01).

843 Data Availability

844 Raw sequencing data are available on the Sequence Read Archive (SRA) database under BioProject:
845 PRJNA739166. This also includes CAGE-seq data aligned to the ASFV-GRG (FR682468.1 *Sus scrofa*
846 (GCF_000003025.6) genomes (see methods above) in BAM format.

847 Acknowledgements

848 The research at UCL was funded in part by the Wellcome Trust (WT 207446/Z/17/Z and WT
849 108877/B/15/Z). For the purpose of Open Access, the author has applied a CC BY public copyright
850 license to any Author Accepted Manuscript version arising from this submission. Research at The
851 Pirbright Institute is funded by the Biotechnology and Biological Sciences Research Council

852 (BBS/E/I/0007030 and BBS/E/I/0007031). The authors are grateful to all members of the RNAP lab and
853 Tine Arnvig for critical reading of the manuscript.

854 References

- 855 1. Gogin A, Gerasimov V, Malogolovkin A, Kolbasov D. African swine fever in the North Caucasus
856 region and the Russian Federation in years 2007-2012. *Virus Res.* 2013 Apr 1;173(1):198–203.
- 857 2. Zhou X, Li N, Luo Y, Liu Y, Miao F, Chen T, et al. Emergence of African Swine Fever in China,
858 2018. *Transbound Emerg Dis.* 2018 Dec 1;65(6):1482–4.
- 859 3. Alonso C, Borca M, Dixon L, Revilla Y, Rodriguez F, Escribano JM, et al. ICTV Virus Taxonomy
860 Profile: Asfarviridae. *J Gen Virol.* 2018 May 1;99(5):613–4.
- 861 4. Koonin E V., Yutin N. Origin and evolution of eukaryotic large nucleo-cytoplasmic DNA viruses.
862 *Intervirology.* 2010;53(5):284–92.
- 863 5. Yutin N, Koonin E V. Hidden evolutionary complexity of Nucleo-Cytoplasmic Large DNA viruses
864 of eukaryotes. *Viol J.* 2012 Aug 14;9(1):161.
- 865 6. Broyles SS. Vaccinia virus transcription. *J Gen Virol.* 2003 Sep 1;84(9):2293–303.
- 866 7. Alejo A, Matamoros T, Guerra M, Andrés G. A proteomic atlas of the African swine fever virus
867 particle. *J Virol.* 2018 Sep 5;JVI.01293-18.
- 868 8. Salas ML, Kuznar J, Viñuela E. Polyadenylation, methylation, and capping of the RNA
869 synthesized in vitro by African swine fever virus. *Virology.* 1981 Sep 1;113(2):484–91.
- 870 9. Rodríguez JM, Salas ML. African swine fever virus transcription. Vol. 173, *Virus Research.*
871 Elsevier B.V.; 2013. p. 15–28.
- 872 10. Cackett G, Matelska D, Sýkora M, Portugal R, Malecki M, Bähler J, et al. The African Swine Fever
873 Virus Transcriptome. *J Virol.* 2020 Feb 19;94(9).
- 874 11. Iyer LM, Balaji S, Koonin E V., Aravind L. Evolutionary genomics of nucleo-cytoplasmic large
875 DNA viruses. *Virus Res.* 2006 Apr;117(1):156–84.
- 876 12. Yutin N, Wolf YI, Raoult D, Koonin E V. Eukaryotic large nucleo-cytoplasmic DNA viruses:
877 clusters of orthologous genes and reconstruction of viral genome evolution. *Viol J.* 2009 Dec
878 17;6(3):223.
- 879 13. Fischer U, Grimm C, Bartuli J, Böttcher B, Szalay A. Structural basis of the complete poxvirus

- 880 transcription initiation process. 2021 Apr 28;
- 881 14. Rodríguez JM, Moreno LT, Alejo A, Lacasta A, Rodríguez F, Salas ML. Genome Sequence of
882 African Swine Fever Virus BA71, the Virulent Parental Strain of the Nonpathogenic and Tissue-
883 Culture Adapted BA71V. Munderloh UG, editor. PLoS One. 2015 Nov 30;10(11):e0142889.
- 884 15. Yáñez RJ, Rodríguez JM, Nogal ML, Yuste L, Enríquez C, Rodríguez JF, et al. Analysis of the
885 complete nucleotide sequence of African swine fever virus. Virology. 1995 Apr 1;208(1):249–
886 78.
- 887 16. Dixon LK, Chapman DAG, Netherton CL, Upton C. African swine fever virus replication and
888 genomics. Virus Res. 2013;173(1):3–14.
- 889 17. Chapman DAG, Tcherepanov V, Upton C, Dixon LK. Comparison of the genome sequences of
890 non-pathogenic and pathogenic African swine fever virus isolates. J Gen Virol. 2008 Feb
891 1;89(2):397–408.
- 892 18. Forth JH, Forth LF, King J, Groza O, Hübner A, Olesen AS, et al. A deep-sequencing workflow for
893 the fast and efficient generation of high-quality African swine fever virus whole-genome
894 sequences. Viruses. 2019;11(9).
- 895 19. Chapman DAG, Darby AC, da Silva M, Upton C, Radford AD, Dixon LK. Genomic analysis of highly
896 virulent Georgia 2007/1 isolate of African swine fever virus. Emerg Infect Dis. 2011
897 Apr;17(4):599–605.
- 898 20. Farlow J, Donduashvili M, Kokhreidze M, Kotorashvili A, Vepkhvadze NG, Kotaria N, et al. Intra-
899 epidemic genome variation in highly pathogenic African swine fever virus (ASFV) from the
900 country of Georgia. Virol J. 2018 Dec 14;15(1):190.
- 901 21. Mazur-Panasiuk N, Woźniakowski G, Niemczuk K. The first complete genomic sequences of
902 African swine fever virus isolated in Poland. Sci Rep. 2019 Dec 1;9(1):3–5.
- 903 22. Granberg F, Torresi C, Oggiano A, Malmberg M, Iscaro C, De Mia GM, et al. Complete genome
904 sequence of an African swine fever virus isolate from Sardinia, Italy. Genome Announc.
905 2016;4(6):1220–36.
- 906 23. Wang Z, Jia L, Li J, Liu H, Liu D. Pan-Genomic Analysis of African Swine Fever Virus. Virologica
907 Sinica. Science Press; 2019. p. 1–4.
- 908 24. Rowlands RJ, Michaud V, Heath L, Hutchings G, Oura C, Vosloo W, et al. African swine fever
29

- 909 virus isolate, Georgia, 2007. *Emerg Infect Dis.* 2008 Dec;14(12):1870–4.
- 910 25. Zhao D, Liu R, Zhang X, Li F, Wang J, Zhang J, et al. Replication and virulence in pigs of the first
911 African swine fever virus isolated in China. *Emerg Microbes Infect.* 2019 Jan 1;8(1):438–47.
- 912 26. Zani L, Forth JH, Forth L, Nurmoja I, Leidenberger S, Henke J, et al. Deletion at the 5'-end of
913 Estonian ASFV strains associated with an attenuated phenotype. *Sci Reports* 2018 81. 2018 Apr
914 25;8(1):1–11.
- 915 27. Gallardo C, Nurmoja I, Soler A, Delicado V, Simón A, Martín E, et al. Evolution in Europe of
916 African swine fever genotype II viruses from highly to moderately virulent. *Vet Microbiol.* 2018
917 Jun 1;219:70–9.
- 918 28. Pershin A, Shevchenko I, Igolkin A, Zhukov I, Mazloum A, Aronova E, et al. A Long-Term Study
919 of the Biological Properties of ASF Virus Isolates Originating from Various Regions of the
920 Russian Federation in 2013–2018. *Vet Sci* 2019, Vol 6, Page 99. 2019 Dec 6;6(4):99.
- 921 29. Sun E, Zhang Z, Wang Z, He X, Zhang X, Wang L, et al. Emergence and prevalence of naturally
922 occurring lower virulent African swine fever viruses in domestic pigs in China in 2020. *Sci China*
923 *Life Sci.* 2021 May 1;64(5):752–65.
- 924 30. Imbery J, Upton C. Organization of the multigene families of African Swine Fever Virus. *Fine*
925 *Focus.* 2017;3(2):155–70.
- 926 31. Netherton CL, Connell S, Benfield CTO, Dixon LK. The Genetics of Life and Death: Virus-Host
927 Interactions Underpinning Resistance to African Swine Fever, a Viral Hemorrhagic Disease.
928 *Front Genet.* 2019 May 3;10(MAY):402.
- 929 32. Reis AL, Abrams CC, Goatley LC, Netherton C, Chapman DG, Sanchez-Cordon P, et al. Deletion
930 of African swine fever virus interferon inhibitors from the genome of a virulent isolate reduces
931 virulence in domestic pigs and induces a protective response. *Vaccine.* 2016 Sep
932 7;34(39):4698–705.
- 933 33. O'Donnell V, Risatti GR, Holinka LG, Krug PW, Carlson J, Velazquez-Salinas L, et al. Simultaneous
934 Deletion of the 9GL and UK Genes from the African Swine Fever Virus Georgia 2007 Isolate
935 Offers Increased Safety and Protection against Homologous Challenge. *J Virol.* 2017 Jan;91(1).
- 936 34. Li D, Zhang J, Yang W, Li P, Ru Y, Kang W, et al. African swine fever virus protein MGF-505-7R
937 promotes virulence and pathogenesis by inhibiting JAK1- and JAK2-mediated signaling. *J Biol*
938 *Chem.* 2021 Nov;297(5):101190.

- 939 35. Li D, Liu YY, Qi X, Wen Y, Li P, Ma Z, et al. African Swine Fever Virus MGF-110-9L-deficient
940 Mutant Has Attenuated Virulence in Pigs. *Virol Sin.* 2021 Apr 1;36(2):187–95.
- 941 36. Keßler C, Forth JH, Keil GM, Mettenleiter TC, Blome S, Karger A. The intracellular proteome of
942 African swine fever virus. *Sci Rep.* 2018 Oct 2;8(1):14714.
- 943 37. Randall RE, Goodbourn S. Interferons and viruses: An interplay between induction, signalling,
944 antiviral responses and virus countermeasures. Vol. 89, *Journal of General Virology.*
945 *Microbiology Society*; 2008. p. 1–47.
- 946 38. Afonso RCL, Piccone ME, Zaffuto KM, Neilan J, Kutish GF, Lu Z, et al. African swine fever virus
947 multigene family 360 and 530 genes affect host interferon response. *J Virol.* 2004;78:1858–64.
- 948 39. Neilan JG, Zsak L, Lu Z, Kutish GF, Afonso CL, Rock DL. Novel Swine Virulence Determinant in
949 the Left Variable Region of the African Swine Fever Virus Genome. *J Virol.* 2002 Apr
950 1;76(7):3095–104.
- 951 40. Golding JP, Goatley L, Goodbourn S, Dixon LK, Taylor G, Netherton CL. Sensitivity of African
952 swine fever virus to type I interferon is linked to genes within multigene families 360 and 505.
953 *Virology.* 2016 Jun 1;493:154–61.
- 954 41. Mosser DM, Edwards JP. Exploring the full spectrum of macrophage activation. Vol. 8, *Nature*
955 *Reviews Immunology.* NIH Public Access; 2008. p. 958–69.
- 956 42. Zhu JJ, Ramanathan P, Bishop EA, O'Donnell V, Gladue DP, Borca M V. Mechanisms of African
957 swine fever virus pathogenesis and immune evasion inferred from gene expression changes in
958 infected swine macrophages. *PLoS One.* 2019;14(11).
- 959 43. Jaing C, Rowland RRR, Allen JE, Certoma A, Thissen JB, Bingham J, et al. Gene expression
960 analysis of whole blood RNA from pigs infected with low and high pathogenic African swine
961 fever viruses. *Sci Rep.* 2017 Dec 31;7(1):10115.
- 962 44. Fan W, Cao Y, Jiao P, Yu P, Zhang H, Chen T, et al. Synergistic effect of the responses of different
963 tissues against African swine fever virus. *Transbound Emerg Dis.* 2021;
- 964 45. Ju X, Li F, Li J, Wu C, Xiang G, Zhao X, et al. Genome-wide transcriptomic analysis of highly
965 virulent African swine fever virus infection reveals complex and unique virus host interaction.
966 *Vet Microbiol.* 2021 Oct 1;261:109211.
- 967 46. Yang B, Shen C, Zhang D, Zhang T, Shi X, Yang J, et al. Mechanism of interaction between virus

- 968 and host is inferred from the changes of gene expression in macrophages infected with African
969 swine fever virus CN/GS/2018 strain. *Virology*. 2021 Dec 1;18(1).
- 970 47. Love MI, Huber W, Anders S. Moderated estimation of fold change and dispersion for RNA-seq
971 data with DESeq2. *Genome Biol.* 2014 Dec 5;15(12):550.
- 972 48. Hammond JM, Kerr SM, Smith GL, Dixon LK. An African swine fever virus gene with homology
973 to DNA ligases. *Nucleic Acids Res.* 1992 Jun 11;20(11):2667–71.
- 974 49. Reis AL, Goatley LC, Jabbar T, Sanchez-Cordon PJ, Netherton CL, Chapman DAG, et al. Deletion
975 of the African Swine Fever Virus Gene DP148R Does Not Reduce Virus Replication in Culture
976 but Reduces Virus Virulence in Pigs and Induces High Levels of Protection against Challenge. *J*
977 *Virology*. 2017 Dec 15;91(24).
- 978 50. Yang Z, Martens CA, Bruno DP, Porcella SF, Moss B. Pervasive initiation and 3'-end formation
979 of poxvirus postreplicative RNAs. *J Biol Chem.* 2012 Sep 7;287(37):31050–60.
- 980 51. Frouco G, Freitas FB, Coelho J, Leitão A, Martins C, Ferreira F. DNA-Binding Properties of African
981 Swine Fever Virus pA104R, a Histone-Like Protein Involved in Viral Replication and
982 Transcription. *J Virology*. 2017;91(12).
- 983 52. Conesa A, Madrigal P, Tarazona S, Gomez-Cabrero D, Cervera A, McPherson A, et al. A survey
984 of best practices for RNA-seq data analysis. *Genome Biol.* 2016 Jan 26;17:13.
- 985 53. García-Escudero R, Viñuela E. Structure of African Swine Fever Virus Late Promoters:
986 Requirement of a TATA Sequence at the Initiation Region. *J Virology*. 2000 Sep 1;74(17):8176–82.
- 987 54. Bailey TL, Boden M, Buske FA, Frith M, Grant CE, Clementi L, et al. MEME SUITE: tools for motif
988 discovery and searching. *Nucleic Acids Res.* 2009 Jul 1;37(Web Server):W202–8.
- 989 55. Gupta S, Stamatoyannopoulos JA, Bailey TL, Noble W. Quantifying similarity between motifs.
990 *Genome Biol.* 2007 Feb 26;8(2):R24.
- 991 56. Rodríguez JM, Salas ML, Viñuela E. Intermediate class of mRNAs in African swine fever virus. *J*
992 *Virology*. 1996 Dec;70(12):8584–9.
- 993 57. Kim DE, Chivian D, Baker D. Protein structure prediction and analysis using the Robetta server.
994 *Nucleic Acids Res.* 2004;32(WEB SERVER ISS.):W526–31.
- 995 58. Vydellingum S, Baylis SA, Bristow C, Smith GL, Dixon LK. Duplicated genes within the variable
996 right end of the genome of a pathogenic isolate of African swine fever virus. *J Gen Virology*. 1993

- 997 Oct 1;74(10):2125–30.
- 998 59. Zhang J, Zhang Y, Chen T, Yang JJ, Yue H, Wang L, et al. Deletion of the L7L-L11L Genes
999 Attenuates ASFV and Induces Protection against Homologous Challenge. *Viruses*. 2021 Feb
1000 1;13(2).
- 1001 60. Krug PW, Holinka LG, O'Donnell V, Reese B, Sanford B, Fernandez-Sainz I, et al. The Progressive
1002 Adaptation of a Georgian Isolate of African Swine Fever Virus to Vero Cells Leads to a Gradual
1003 Attenuation of Virulence in Swine Corresponding to Major Modifications of the Viral Genome.
1004 *J Virol*. 2015 Feb 15;89(4):2324–32.
- 1005 61. Kelley LA, Mezulis S, Yates CM, Wass MN, Sternberg MJE. The Phyre2 web portal for protein
1006 modeling, prediction and analysis. *Nat Protoc*. 2015 May 7;10(6):845–58.
- 1007 62. Liu H, Li L, Voss C, Wang F, Liu J, Li SSC. A Comprehensive Immunoreceptor Phosphotyrosine-
1008 based Signaling Network Revealed by Reciprocal Protein–Peptide Array Screening. *Mol Cell*
1009 *Proteomics*. 2015 Jul 1;14(7):1846–58.
- 1010 63. Gabler F, Nam SZ, Till S, Mirdita M, Steinegger M, Söding J, et al. Protein Sequence Analysis
1011 Using the MPI Bioinformatics Toolkit. *Curr Protoc Bioinforma*. 2020 Dec 1;72(1).
- 1012 64. Robert C, Kapetanovic R, Beraldi D, Watson M, Archibald AL, Hume DA. Identification and
1013 annotation of conserved promoters and macrophage-expressed genes in the pig genome. *BMC*
1014 *Genomics*. 2015 Nov 18;16(1).
- 1015 65. Ganchi PA, Sun SC, Greene WC, Ballard DW. A novel NF-kappa B complex containing p65
1016 homodimers: implications for transcriptional control at the level of subunit dimerization. *Mol*
1017 *Cell Biol*. 1993 Dec;13(12):7826–35.
- 1018 66. Dixon LK, Abrams CC, Bowick G, Goatley LC, Kay-Jackson PC, Chapman D, et al. African swine
1019 fever virus proteins involved in evading host defence systems. In: *Veterinary Immunology and*
1020 *Immunopathology*. 2004. p. 117–34.
- 1021 67. Powell PP, Dixon LK, Parkhouse RM. An IkappaB homolog encoded by African swine fever virus
1022 provides a novel mechanism for downregulation of proinflammatory cytokine responses in
1023 host macrophages. *J Virol*. 1996;70(12):8527–33.
- 1024 68. Granja AG, Sánchez EG, Sabina P, Fresno M, Revilla Y. African swine fever virus blocks the host
1025 cell antiviral inflammatory response through a direct inhibition of PKC-theta-mediated p300
1026 transactivation. *J Virol*. 2009 Jan 15;83(2):969–80.

- 1027 69. Nogal ML, González de Buitrago G, Rodríguez C, Cubelos B, Carrascosa AL, Salas ML, et al.
1028 African swine fever virus IAP homologue inhibits caspase activation and promotes cell survival
1029 in mammalian cells. *J Virol.* 2001 Mar 15;75(6):2535–43.
- 1030 70. Takeya T, Hanafusa H. DNA sequence of the viral and cellular src gene of chickens. II.
1031 Comparison of the src genes of two strains of avian sarcoma virus and of the cellular homolog.
1032 *J Virol.* 1982;44(1):12–8.
- 1033 71. Kaneko T, Stogios PJ, Ruan X, Voss C, Evdokimova E, Skarina T, et al. Identification and
1034 characterization of a large family of superbinding bacterial SH2 domains. *Nat Commun.* 2018
1035 Dec 1;9(1).
- 1036 72. Liu Y, Li Y, Xie Z, Ao Q, Di D, Yu W, et al. Development and in vivo evaluation of MGF100-1R
1037 deletion mutant in an African swine fever virus Chinese strain. *Vet Microbiol.* 2021 Oct 1;261.
- 1038 73. Vuono E, Ramirez-Medina E, Pruitt S, Rai A, Silva E, Espinoza N, et al. Evaluation in swine of a
1039 recombinant georgia 2010 african swine fever virus lacking the i8l gene. *Viruses.* 2021 Jan
1040 1;13(1).
- 1041 74. Camacho A, Viñuela E. Protein p22 of African swine fever virus: An early structural protein that
1042 is incorporated into the membrane of infected cells. *Virology.* 1991 Mar 1;181(1):251–7.
- 1043 75. Netherton C, Rouiller I, Wileman T. The subcellular distribution of multigene family 110
1044 proteins of African swine fever virus is determined by differences in C-terminal KDEL
1045 endoplasmic reticulum retention motifs. *J Virol.* 2004 Apr 1;78(7):3710–21.
- 1046 76. Ramirez-Medina E, Vuono E, Pruitt S, Rai A, Silva E, Espinoza N, et al. Development and In Vivo
1047 Evaluation of a MGF110-1L Deletion Mutant in African Swine Fever Strain Georgia. *Viruses.*
1048 2021 Feb 1;13(2).
- 1049 77. Cackett G, Sýkora M, Werner F. Transcriptome view of a killer: African swine fever virus. Vol.
1050 48, *Biochemical Society Transactions.* Portland Press Ltd; 2020. p. 1569–81.
- 1051 78. Quintas A, Pérez-Núñez D, Sánchez EG, Nogal ML, Hentze MW, Castelló A, et al.
1052 Characterization of the African Swine Fever Virus Decapping Enzyme during Infection. Jung JU,
1053 editor. *J Virol.* 2017 Dec 15;91(24):e00990-17.
- 1054 79. Kunsch C, Ruben SM, Rosen CA. Selection of optimal kappa B/Rel DNA-binding motifs:
1055 interaction of both subunits of NF-kappa B with DNA is required for transcriptional activation.
1056 *Mol Cell Biol.* 1992 Oct;12(10):4412–21.

- 1057 80. Gómez del Moral M, Ortuño E, Fernández-Zapatero P, Alonso F, Alonso C, Ezquerro A, et al.
1058 African Swine Fever Virus Infection Induces Tumor Necrosis Factor Alpha Production:
1059 Implications in Pathogenesis. *J Virol*. 1999 Mar 1;73(3):2173–80.
- 1060 81. Roy S, Schmeier S, Arner E, Alam T, Parihar SP, Ozturk M, et al. Redefining the transcriptional
1061 regulatory dynamics of classically and alternatively activated macrophages by deepCAGE
1062 transcriptomics. *Nucleic Acids Res*. 2015;43(14):6969–82.
- 1063 82. Castelló A, Quintas A, Sánchez EG, Sabina P, Nogal M, Carrasco L, et al. Regulation of host
1064 translational machinery by African swine fever virus. *PLoS Pathog*. 2009 Aug;5(8):e1000562.
- 1065 83. Sánchez EG, Quintas A, Nogal M, Castelló A, Revilla Y. African swine fever virus controls the
1066 host transcription and cellular machinery of protein synthesis. *Virus Res*. 2013 Apr 1;173(1):58–
1067 75.
- 1068 84. Barrado-Gil L, Del Puerto A, Muñoz-Moreno R, Galindo I, Cuesta-Geijo MA, Urquiza J, et al.
1069 African Swine Fever Virus Ubiquitin-Conjugating Enzyme Interacts With Host Translation
1070 Machinery to Regulate the Host Protein Synthesis. *Front Microbiol*. 2020 Dec 15;11.
- 1071 85. Gschwandtner M, Derler R, Midwood KS. More Than Just Attractive: How CCL2 Influences
1072 Myeloid Cell Behavior Beyond Chemotaxis. *Front Immunol*. 2019 Dec 13;0:2759.
- 1073 86. Xia C, Braunstein Z, Toomey AC, Zhong J, Rao X. S100 proteins as an important regulator of
1074 macrophage inflammation. Vol. 8, *Frontiers in Immunology*. Frontiers Media S.A.; 2018.
- 1075 87. Yang Z, Bruno DP, Martens CA, Porcella SF, Moss B. Simultaneous high-resolution analysis of
1076 vaccinia virus and host cell transcriptomes by deep RNA sequencing. *Proc Natl Acad Sci U S A*.
1077 2010 Jun 22;107(25):11513–8.
- 1078 88. Olasz F, Tombácz D, Torma G, Csabai Z, Moldován N, Dörmő Á, et al. Short and Long-Read
1079 Sequencing Survey of the Dynamic Transcriptomes of African Swine Fever Virus and the Host
1080 Cells. *Front Genet*. 2020 Jul 28;11:2020.02.27.967695.
- 1081 89. Torma G, Tombácz D, Csabai Z, Moldován N, Mészáros I, Zádori Z, et al. Combined short and
1082 long-read sequencing reveals a complex transcriptomic architecture of African swine fever
1083 virus. *Viruses*. 2021 Apr 1;13(4).
- 1084 90. Yang Z, Bruno DP, Martens CA, Porcella SF, Moss B. Genome-Wide Analysis of the 5' and 3'
1085 Ends of Vaccinia Virus Early mRNAs Delineates Regulatory Sequences of Annotated and
1086 Anomalous Transcripts. *J Virol*. 2011 Jun;85(12):5897–909.

- 1087 91. Gershon PD, Moss B. Early transcription factor subunits are encoded by vaccinia virus late
1088 genes. *Proc Natl Acad Sci U S A*. 1990 Jun 1;87(11):4401–5.
- 1089 92. Li J, Broyles SS. Recruitment of vaccinia virus RNA polymerase to an early gene promoter by
1090 the viral early transcription factor. *J Biol Chem*. 1993;268(4):2773–80.
- 1091 93. Patikoglou GA, Kim JL, Sun L, Yang SH, Kodadek T, Burley SK. TATA element recognition by the
1092 TATA box-binding protein has been conserved throughout evolution. *Genes Dev*. 1999 Dec
1093 15;13(24):3217–30.
- 1094 94. Andrews S. FastQC A Quality Control tool for High Throughput Sequence Data. Babraham,
1095 England: Babraham Bioinformatics;
- 1096 95. Langmead B, Salzberg SL. Fast gapped-read alignment with Bowtie 2. *Nat Methods*. 2012 Apr
1097 4;9(4):357–9.
- 1098 96. Kim D, Langmead B, Salzberg SL. HISAT: a fast spliced aligner with low memory requirements.
1099 *Nat Methods*. 2015 Apr 9;12(4):357–60.
- 1100 97. Quinlan AR, Hall IM. BEDTools: a flexible suite of utilities for comparing genomic features.
1101 *Bioinformatics*. 2010 Mar 15;26(6):841–2.
- 1102 98. RStudio Team. RStudio: Integrated Development for R. Boston, MA: RStudio, Inc; 2016.
- 1103 99. Huber W, Carey VJ, Gentleman R, Anders S, Carlson M, Carvalho BS, et al. Orchestrating high-
1104 throughput genomic analysis with Bioconductor. *Nat Methods*. 2015 Feb 1;12(2):115–21.
- 1105 100. Thodberg M, Thieffry A, Vitting-Seerup K, Andersson R, Sandelin A. CAGEfightR: Analysis of 5'-
1106 end data using R/Bioconductor. *BMC Bioinformatics*. 2019 Oct 4;20(1):487.
- 1107 101. Anders S, Pyl PT, Huber W. HTSeq—a Python framework to work with high-throughput
1108 sequencing data. *Bioinformatics*. 2015 Jan 15;31(2):166–9.
- 1109 102. Upton C, Slack S, Hunter AL, Ehlers A, Roper RL, Rock DL. Poxvirus orthologous clusters: toward
1110 defining the minimum essential poxvirus genome. *J Virol*. 2003 Jul 1;77(13):7590–600.
- 1111 103. Tu SL, Upton C. Bioinformatics for Analysis of Poxvirus Genomes. In: *Methods in Molecular*
1112 *Biology*. Humana Press Inc.; 2019. p. 29–62.
- 1113 104. DP K, SM R, GH H, SS G, PJ W, LK D, et al. Development of a TaqMan PCR assay with internal
1114 amplification control for the detection of African swine fever virus. *J Virol Methods*. 2003
1115 Jan;107(1):53–61.

- 1116 105. Melchjorsen J, Kristiansen H, Christiansen R, Rintahaka J, Matikainen S, Paludan SR, et al.
1117 Differential regulation of the OASL and OAS1 genes in response to viral infections. *J Interf*
1118 *Cytokine Res.* 2009 Apr 1;29(4):199–207.
- 1119 106. Bailey TL, Elkan C. Fitting a mixture model by expectation maximization to discover motifs in
1120 biopolymers. *Proceedings Int Conf Intell Syst Mol Biol.* 1994;2:28–36.
- 1121 107. Ohmiya H, Vitezic M, Frith MC, Itoh M, Carninci P, Forrest ARR, et al. RECLU: A pipeline to
1122 discover reproducible transcriptional start sites and their alternative regulation using capped
1123 analysis of gene expression (CAGE). *BMC Genomics.* 2014 Apr 25;15(1):269.
- 1124 108. Robinson MD, McCarthy DJ, Smyth GK. edgeR: A Bioconductor package for differential
1125 expression analysis of digital gene expression data. *Bioinformatics.* 2009 Nov 11;26(1):139–40.
- 1126 109. Huang DW, Sherman BT, Lempicki RA. Systematic and integrative analysis of large gene lists
1127 using DAVID bioinformatics resources. *Nat Protoc.* 2009;4(1):44–57.
- 1128 110. Altschul SF, Gish W, Miller W, Myers EW, Lipman DJ. Basic local alignment search tool. *J Mol*
1129 *Biol.* 1990 Oct 5;215(3):403–10.
- 1130 111. Bateman A. UniProt: A worldwide hub of protein knowledge. *Nucleic Acids Res.* 2019 Jan
1131 8;47(D1):D506–15.
- 1132 112. Ramírez F, Dündar F, Diehl S, Grüning BA, Manke T. deepTools: a flexible platform for exploring
1133 deep-sequencing data. *Nucleic Acids Res.* 2014 Jul;42(Web Server issue):W187-91.
- 1134 113. Crooks GE, Hon G, Chandonia JM, Brenner SE. WebLogo: A sequence logo generator. *Genome*
1135 *Res.* 2004 May 12;14(6):1188–90.
- 1136 114. Grant CE, Bailey TL, Noble WS. FIMO: scanning for occurrences of a given motif. *Bioinformatics.*
1137 2011 Apr 1;27(7):1017–8.
- 1138 115. McCarthy DJ, Chen Y, Smyth GK. Differential expression analysis of multifactor RNA-Seq
1139 experiments with respect to biological variation. *Nucleic Acids Res.* 2012 May 1;40(10):4288–
1140 97.
- 1141 116. Benjamini Y, Hochberg Y. Controlling the False Discovery Rate: A Practical and Powerful
1142 Approach to Multiple Testing. *J R Stat Soc Ser B.* 1995 Jan;57(1):289–300.
- 1143 117. Yates AD, Achuthan P, Akanni W, Allen J, Allen J, Alvarez-Jarreta J, et al. Ensembl 2020. *Nucleic*
1144 *Acids Res.* 2020 Jan 1;48(D1):D682–8.

1145 118. Wheeler DL, Church DM, Federhen S, Lash AE, Madden TL, Pontius JU, et al. Database resources
1146 of the National Center for Biotechnology. *Nucleic Acids Res.* 2003 Jan 1;31(1):28–33.

1147

1148 Figures

1149

1150 Figure 1. Functional genome annotation of ASFV GRG. (a) Comparison between the genomes of BA71V
1151 and GRG, generated with Circos (<http://circos.ca/>). Blue lines represent sequence conservation (Blast
1152 E-values per 100 nt). The Inner ring represents genes defined as MGF members (purple), and all others
1153 (grey). The outer ring shows annotated genes which we have defined as early or late according to
1154 downregulation or upregulation between 5 hpi and 16 hpi from DESeq2 analysis. (b) 189 GRG
1155 annotated ORFs are represented as arrows and coloured according to strand. CAGE-seq peaks across
1156 the GRG genome at 5 hpi (c) and 16 hpi (d), normalized coverage reads per million mapped reads
1157 (RPM) of 5' ends of CAGE-seq reads. The coverage was capped at 20000 RPM for visualisation, though
1158 multiple peaks exceeded this. DeepTools (112), was used to convert bam files to bigwig format and
1159 imported into Rstudio for visual representation via packages ggplot, ggbio, rtracklayer, and gggenes
1160 was used to generate the ORF map in (b).

1161

1162 Figure 2. Summary of GRG gene expression (a) Expression profiles for 164 genes for which we
1163 annotated pTSSs from CAGE-seq and which showed significant differential expression. Log₂ fold
1164 change and basemean expression values were from DESeq2 analysis of raw counts (see methods).
1165 Genes are coloured according to their log₂ fold change in expression as red (positive: upregulated
1166 from 5 hpi to 16 hpi) or blue (negative: downregulated). MGFs are emphasised with a black outline to
1167 highlight their overrepresentation in the group of downregulated genes. (b) Expression profiles for 41
1168 genes (excluding nORFs) only detected as being expressed in GRG and not BA71V, format as in (a). (c)
1169 Expression (RPM) of 20 highest-expressed genes at 5 hpi, error bars represent standard deviation
1170 between replicates. (d) Expression (RPM) of 20 highest-expressed genes at 16 hpi pi, error bars are
1171 the standard deviation between replicates.

1172

1173 Figure 3. Comparison of gene expression profiles for genes shared between GRG and BA71V. Scatter
1174 plots of mean RPM across replicates for shared genes at 5 hpi (a) and 16 hpi (b), coloured according
1175 to whether genes show significant downregulation (blue), or upregulation (red) according to DESeq2
38

1176 analysis in GRG. In both (b) and (c) genes with RPM values above 40000 RPM in either strain are
1177 labelled. (c) Comparison of log₂ fold change in expression values of genes in GRG and BA71V, in blue
1178 are downregulated (early) genes in both strains, red are upregulated (late) genes in both strains, while
1179 the genes which disagree in their differential expression patterns between strains are in black. R
1180 represents the Pearson Correlation coefficient for each individual plot in (a), (b), and (c). Due to
1181 inconsistencies in their genome annotations, two genes were omitted from the BA71V-GRG
1182 transcriptome comparisons in Figures 2b and 3a-d: EP296R in GRG known as E296R in BA71V, and
1183 C122R (GRG) is the old nomenclature for C105R (BA71V), which are now correctly named in
1184 Supplementary Table 1e and Figure 2a. Both genes showed the same early expression patterns in
1185 BA71V (10) and GRG (Supplementary Table 1e) so would strengthen the patterns observed.

1186

1187 Figure 4. Increase in virus genome copy number mRNA levels during late infection. (a) The 'log₂
1188 change' represents log₂ of the ratio of CAGE-seq reads (normalised per million mapped reads) at 16
1189 hpi vs. 5 hpi per nucleotide across the genome. Alignment comparisons and calculations were done
1190 with deepTools (112). (b) Replicate means of CAGE-seq reads mapped to either the BA71V (green) or
1191 GRG (purple) genomes throughout infection. (c) Fold change in CAGE-seq reads during infection,
1192 calculated via mean value across 2 replicates, but with the assumption number of reads at 0 hpi is 0,
1193 therefore dividing by values from 5 hpi. (d) Change in genome copies from DNA qPCR of B646L gene,
1194 dividing by value at 0 hpi to represent '1 genome copy per infected cell'. (e) Fold change in genome
1195 copies present at 0 hpi, 5 hpi and 16 hpi from qPCR in (d). (d) calculated as for (c), but with actual
1196 values for 0 hpi.

1197

1198 Figure 5. RT-PCR results of genes for comparison to CAGE-seq data from (a) MGF 505-7R, (b) NP419L,
1199 (c) D345L, (d) MGF 360-12L, (e) MGF 505-9R, and (f) qRT-PCR results of C315R (ASFV-TFIIB). (NT = no
1200 template control). For each panel at the top is a diagrammatic representation of each gene's TSSs
1201 (bent arrow, including both pTSS and ioTSSs), annotated ORF (red arrow), and arrow pairs in cyan or
1202 yellow represent the primers used for PCR (see methods for primer sequences). Beneath each PCR
1203 results are bar charts representing the CAGE-seq results as either normalised (mean RPM) or raw
1204 (mean read counts) data, error bars show the range of values from each replicate.

1205

1206 Figure 6. Comparison of the raw read counts for genes shared between BA71V and GRG. (a) clustered
1207 heatmap representation of raw counts for genes shared between BA71V and GRG, generated with
1208 pheatmap. (b) broad patterns represented by genes in the 5 clusters indicated in (a). (c) histogram
1209 showing the percentage of the total raw reads per gene which are detected at 16 hpi vs. 5 hpi post-
1210 infection, and comparing the distribution of percentages between GRG and BA71V. (d) Mean read
1211 counts from GRG at 5 hpi vs 16 hpi replicates, showing a significant increase (T-test, p-value: 0.045)
1212 from 5 hpi to 16 hpi.

1213

1214 Figure 7. Promoter motifs and initiators detected in early and late ASFV GRG TSSs including alternative
1215 TSSs and those for nORFs. (a) Consensus of 30 bp upstream and 5 bp downstream of all 134 early TSSs
1216 including nORFs, with the conserved EPM (10) and Inr annotated. (b) 30 bp upstream and 5 bp
1217 downstream of all 234 late gene and nORFs TSSs, with the LPM and Inr annotated (c) The conserved
1218 EPM detected via MEME motif search of 35 bp upstream for 133 for 134 early TSSs (E-value: 3.1e-
1219 069). The conserved LPM detected via MEME motif search of 35 bp upstream for 46 for 234 late gene
1220 TSSs (E-value: 2.6e-003). The locations of the EPM shown in (b) and LPM shown in (d) are annotated
1221 with brackets in (a) and (b), respectively. Motifs detected via MEME search of 35 bp upstream of genes
1222 in clusters from Figure 6: cluster 1 (7 genes, E-value: 9.1e-012), 2 (15 genes, E-value: 2.6e-048), 3 (60
1223 genes, E-value: 1.0e-167), 4 (32 genes, E-value: 4.7e-105), 5 (16 genes, E-value: 5.7e-036), are shown
1224 in e-i, respectively. For ease of comparison, (e), (g), (i) and (f), (h) are aligned at TSS position. All motifs
1225 were generated using Weblogo 3 (113). (k) shows the distribution of MEME motif-end distances, from
1226 last nt (in coloured bracket), to their respective downstream TSSs.

1227

1228 Figure 8. The TSSs of MGF 360-19R. Panels (a) 5 hpi and (b) 16 hpi show CAGE-seq 5' end data from
1229 these time-points, in red are reads from the plus strand and blue from the minus strand, the RPM
1230 scales are on the right. (c) TSSs are annotated with arrows if they can generate a minimum of 5 residue-
1231 ORF downstream, and grey bars indicate where they are located on the CAGE-seq coverage in (a) and
1232 (b). ORFs identified downstream of TSSs are shown as red arrows (visualized with R package gggenes),
1233 including three short nORFs out of frame with MGF 360-19R. Also shown are three in-frame truncation
1234 variants, from TSSs detected inside the full-length MGF 360-19R 269-residue ORF, downstream of its
1235 pTSS at 185213. Blue or yellow boxes upstream of TSSs indicate whether the EPM or LPM
1236 (respectively) could be detected within 35 nt upstream of the TSS using FIMO searching (114).

1237

1238 Figure 9. Summary of intra-ORF TSSs (ioTSSs) and nORFs detected in the GRG genome, further
1239 information in Supplementary Table 2. (a) Summarises the gene types in which ioTSSs were detected,
1240 showing an overrepresentation of MGFs, especially from families 360 and 505, furthermore, the
1241 majority of ioTSSs are detected at 16 hpi. (b) For ioTSSs in-frame with the original, summarised are
1242 the subsequent UTR lengths i.e. distance from TSS to next in frame ATG start codon, which could
1243 generate a truncation variant. (c) Example of a miss-annotation for CP204L, whereby the pTSS is
1244 downstream the predicted start codon. (d) and (e) show the results of 5'RACE for three genes (DP146L,
1245 pNG4, and CP204L, see methods for primers), at 5 hpi and 16 hpi, respectively. Examples of genome
1246 regions around DP146L (f) and pNG4 (g), wherein ioTSSs were detected with capacity for altering ORF
1247 length in subsequent transcripts, and therefore protein output. Primers used for 5'RACE for DP146L
1248 and pNG4 are represented as black arrows in (f) and (g), respectively.

1249

1250 Figure 10. MGF 100 genes likely encode SH2-domain factors. (a) Occurrence of MGF 100 genes in
1251 selected ASFV strains, with genotype and pathogenicity indicated (as yes, Y, or no, N). '1L/2L' refers to
1252 the gene MGF 100-2L (DP141L in BA71V) and MGF 100-1L in the FR682468.1 genome annotation. (b)
1253 The top panel illustrates representative SH2 domain structures (Suppressor of Cytokine Signalling 1
1254 and -2 and the PI3K alpha), and the bottom shows structural homology models of MGF 100 members
1255 1L, 1R, and I7L and I8L superimposed. The PHYRE2 algorithm (56) was used to predict models for MGF
1256 100 members (Supplementary Table 2d), and the structures at the top were detected as the top hits
1257 for each of the MGF 100 models shown in the lower panel. (c) Structure-guided multiple sequence
1258 alignment of selected MGF 100 member models, alongside known SH2 domain structures (annotated
1259 as SH2_name_PDB number).

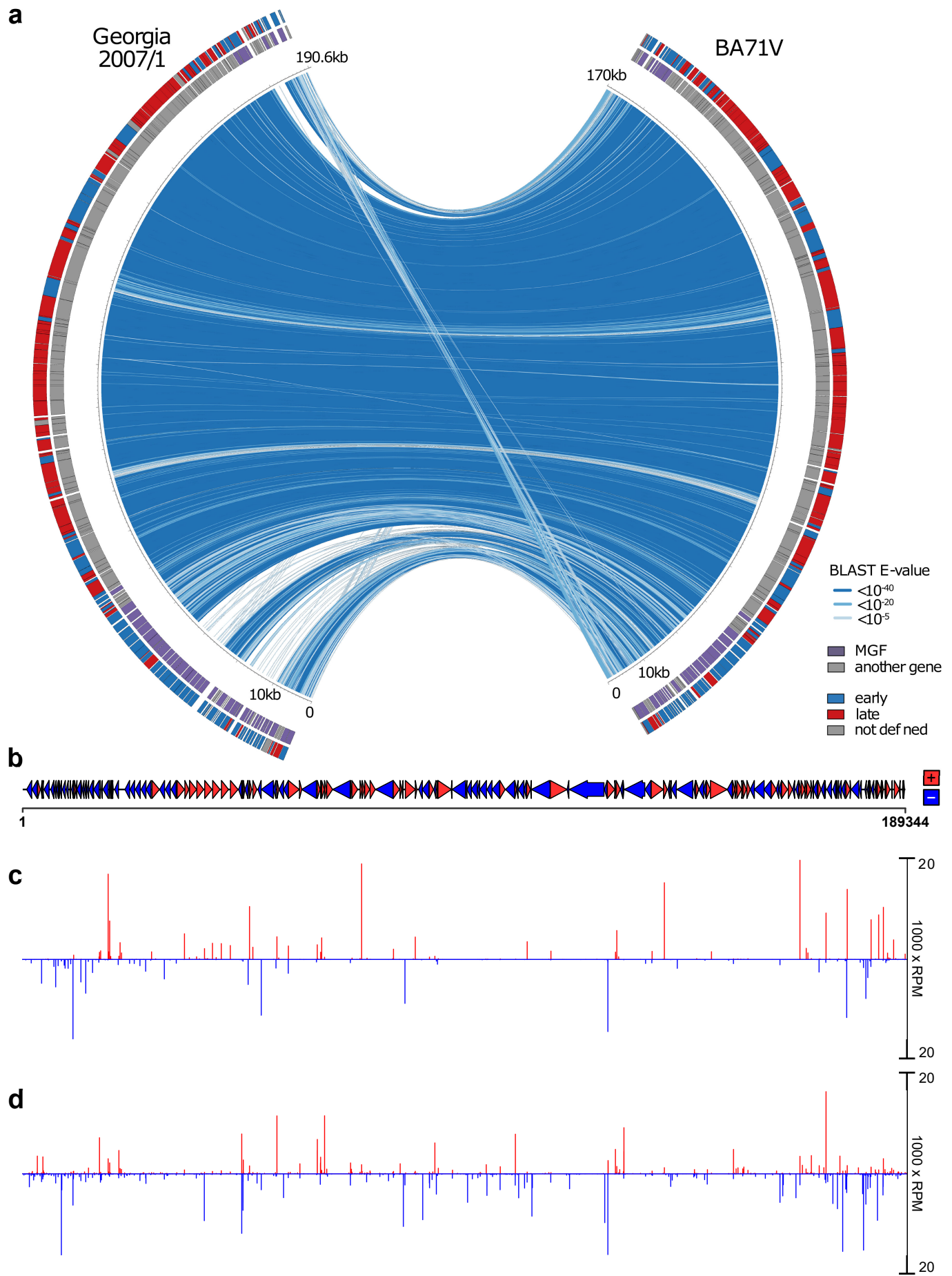
1260

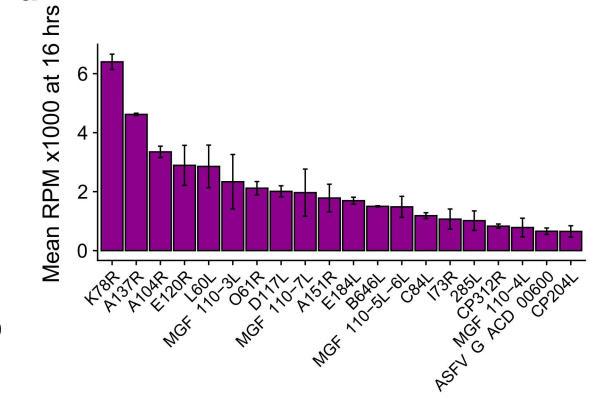
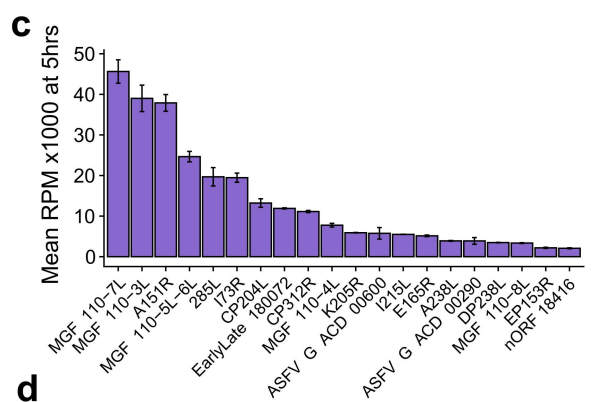
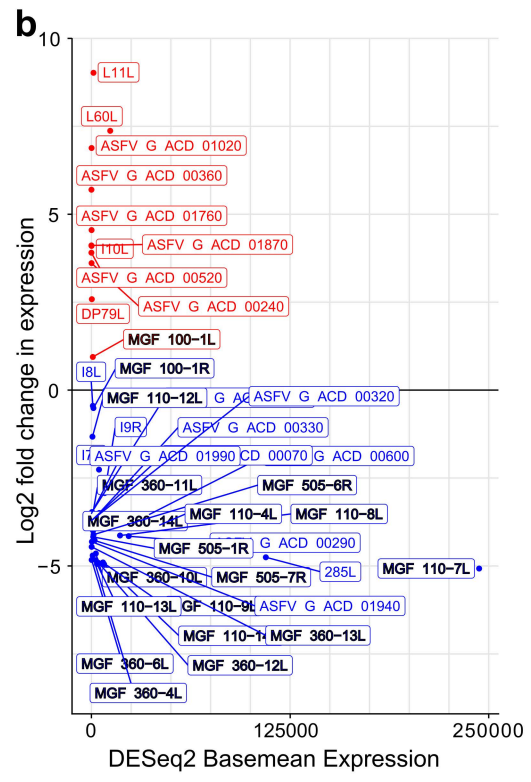
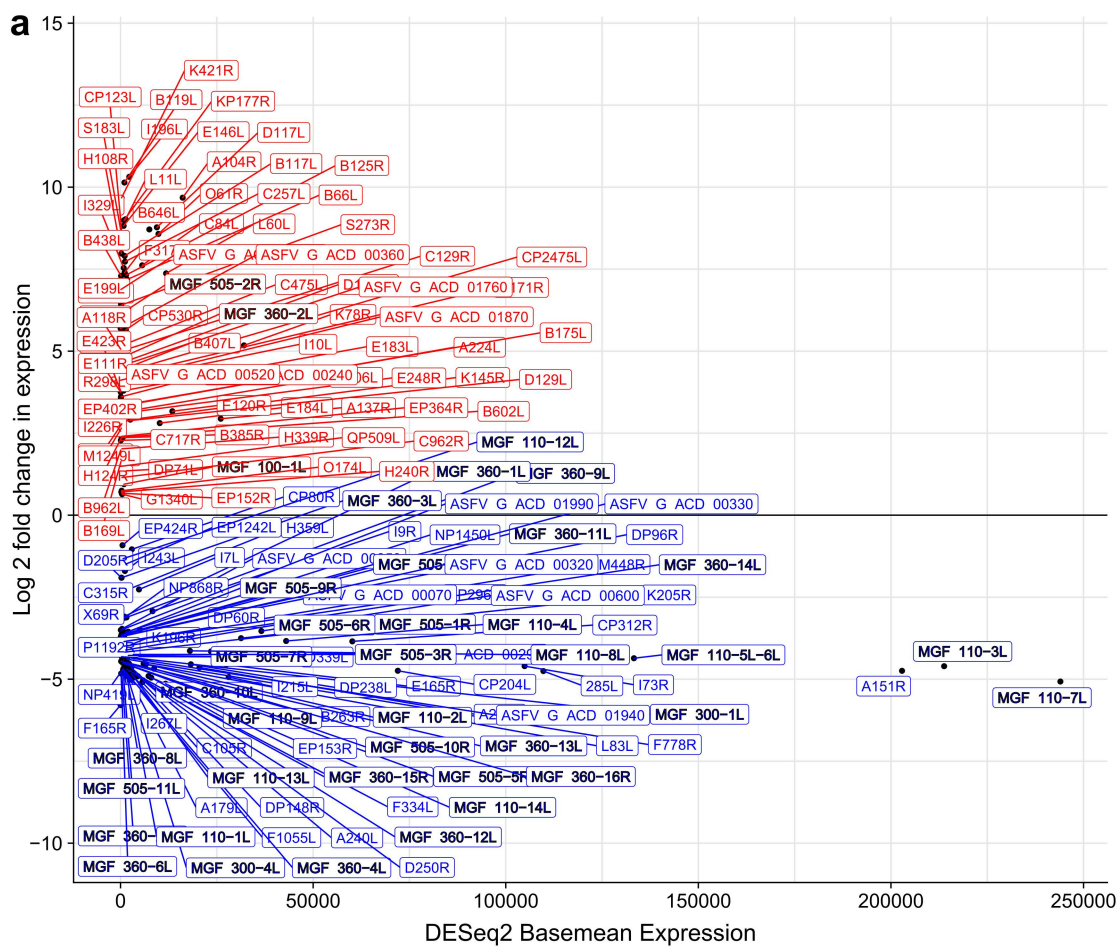
1261 Figure 11. Changes in the swine macrophage transcriptome upon ASFV GRG infection. (a) Major
1262 expression response profiles of the pig macrophage transcriptome. Late response genes are
1263 significantly deregulated (false discovery rate < 0.05) in one direction both between mock-infected
1264 (ctrl) and 16 hpi as well as between 5 and 16 hpi, but not between mock-infected and 5 hpi. Early
1265 response genes are significantly deregulated in one direction both between ctrl and 5 hpi as well as
1266 ctrl and 16 hpi, but not between 5 and 16 hpi. (b) Relationship of log fold changes (logFC) of TSS-
1267 derived gene expression levels of the total 9,384 swine genes expressed in macrophages between 5-
1268 16 hpi and ctrl-16 hpi. Colors correspond to the response groups from the panel a. (c) Relationship of
1269 log fold changes of TSS-derived gene expression levels of the total 9,384 swine genes expressed in

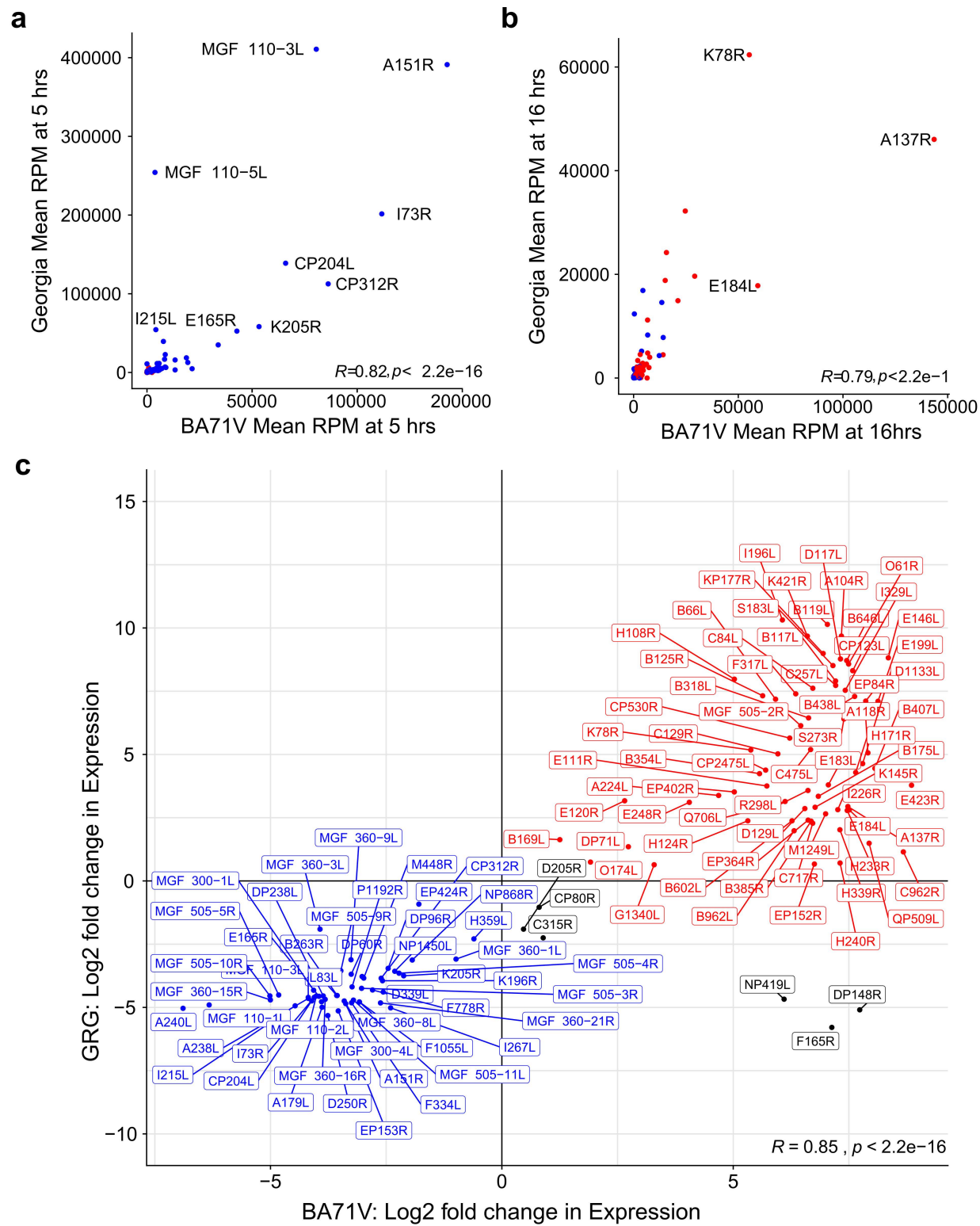
1270 macrophages between 5–16 hpi and ctrl–5 hpi. (d) MA plot of the TSS-derived gene expression levels
1271 between 5 and 16 hpi based on differential expression analysis with edgeR (108,115). (e)
1272 Representative overrepresented functional annotations of the upregulated (red) and downregulated
1273 (blue) macrophage genes following late transcription response (Benjamini-corrected p-value lower
1274 than 0.05). Numbers on the right to the bars indicate total number of genes from a given group
1275 annotated with a given annotation. (f) RT-PCR of four genes of interest indicated in (d). 'C' is the
1276 uninfected macrophage control, NTC is the Non Template Control for each PCR, excluding template
1277 DNA. See methods for primers used.

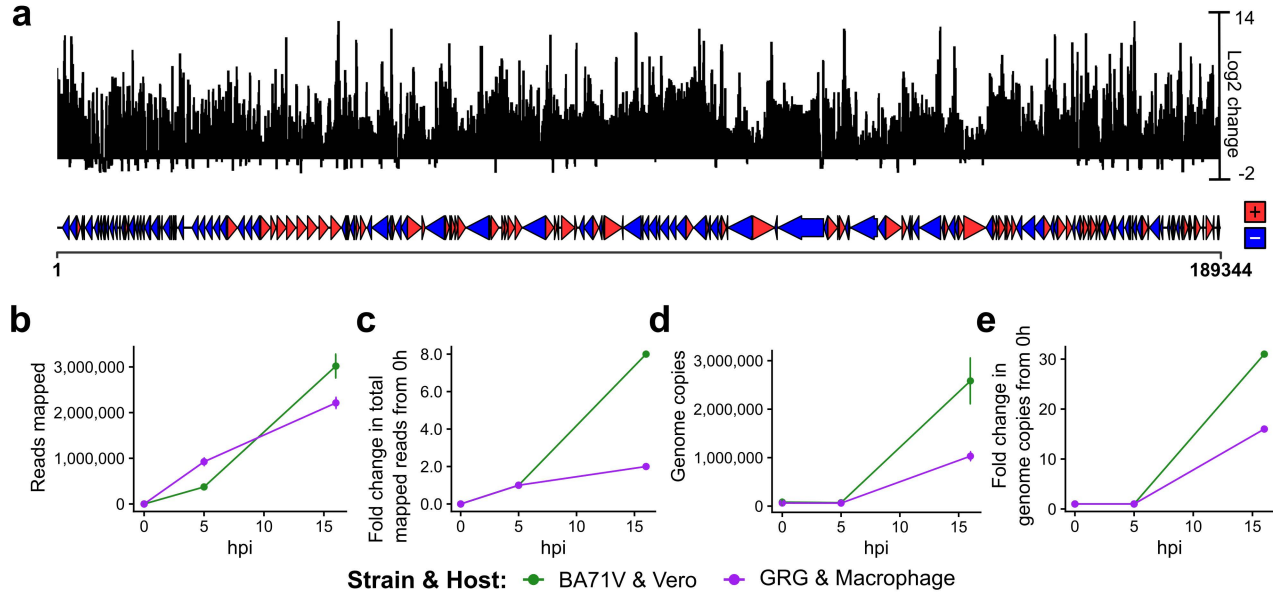
1278

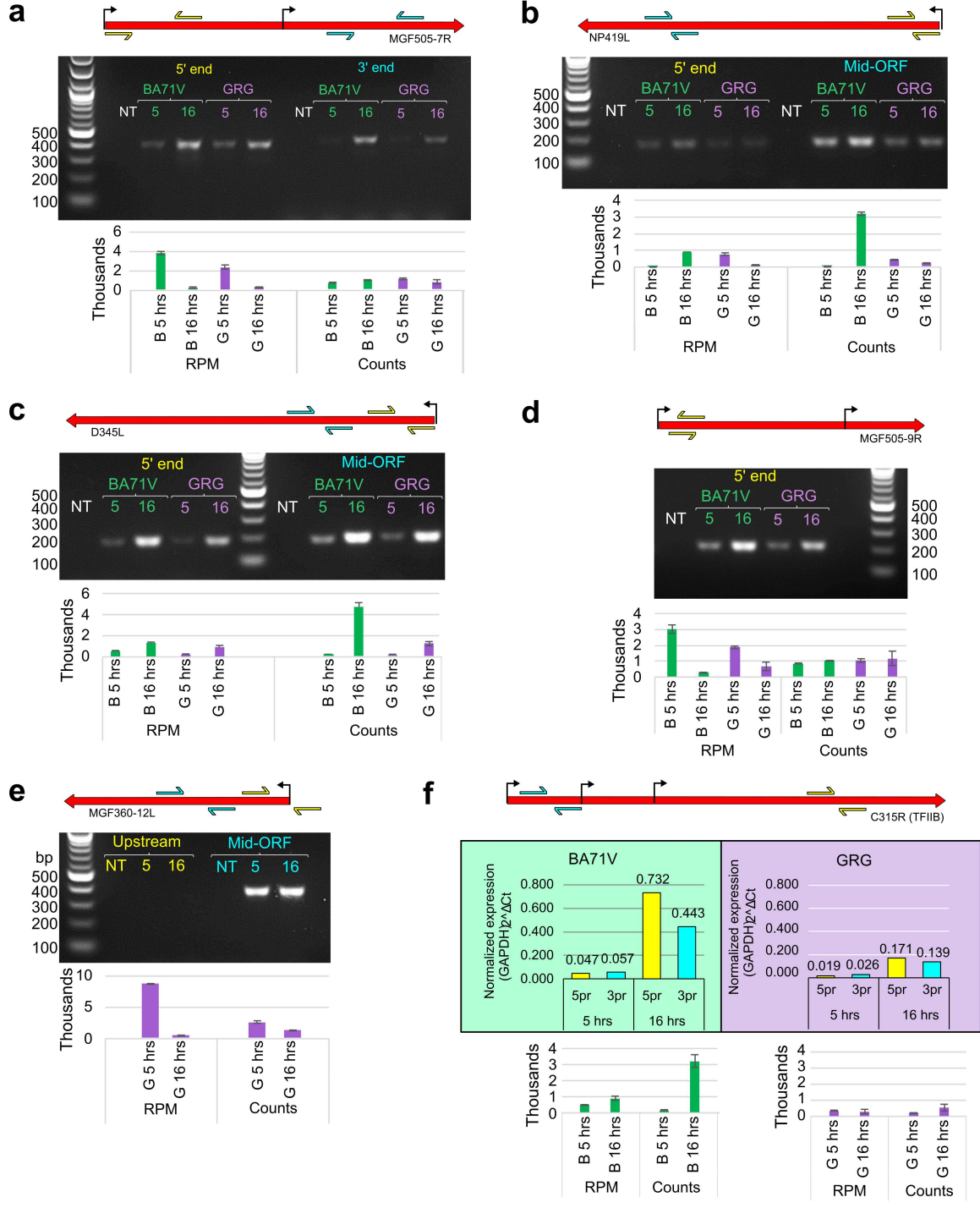
1279 Figure 12. Protein expression at different times during infection of swine macrophages with ASFV-
1280 GRG. Two different batches of macrophages (S1 and S2) were infected with MOI 5 or left uninfected
1281 as a control (Ctrl) and at 0, 5 and 16hpi cellular extracts were collected and analysed via SDS-PAGE
1282 Western blot for the presence of ISG15 and γ -Tubulin as a protein loading control (a) and for the
1283 presence of viral protein P30 as control of ASFV infection (b). (c), (d) and (e) are the results from ELISAs
1284 for detection of porcine TNF- α , IL-8/CXCL8, and CCL2/MCP-1, respectively, in culture supernatants.
1285 Results are presented as 'Relative to control' values (y-axis of c-e) calculated by performing ELISAs in
1286 parallel for control and GRG infection at each timepoint.

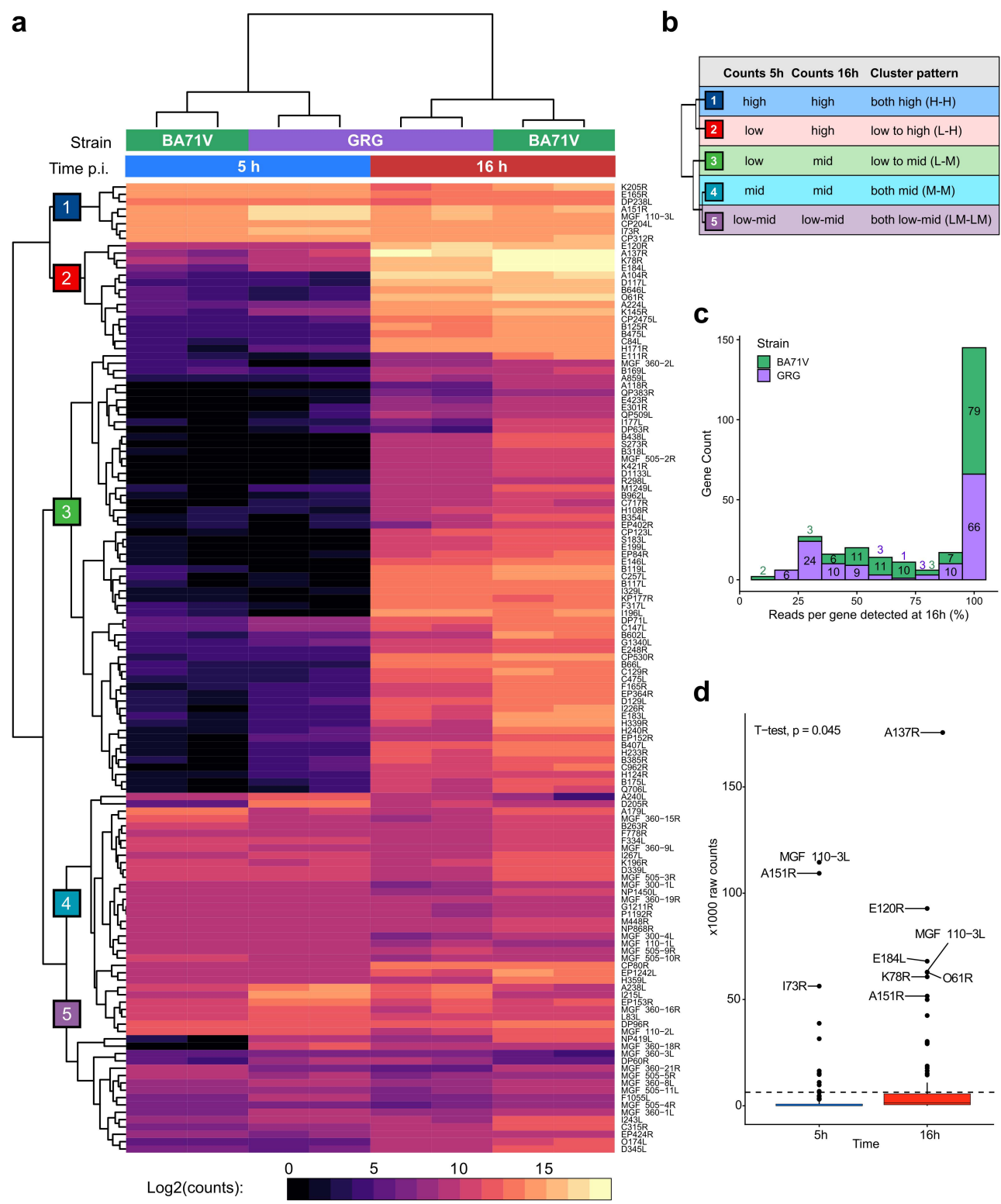


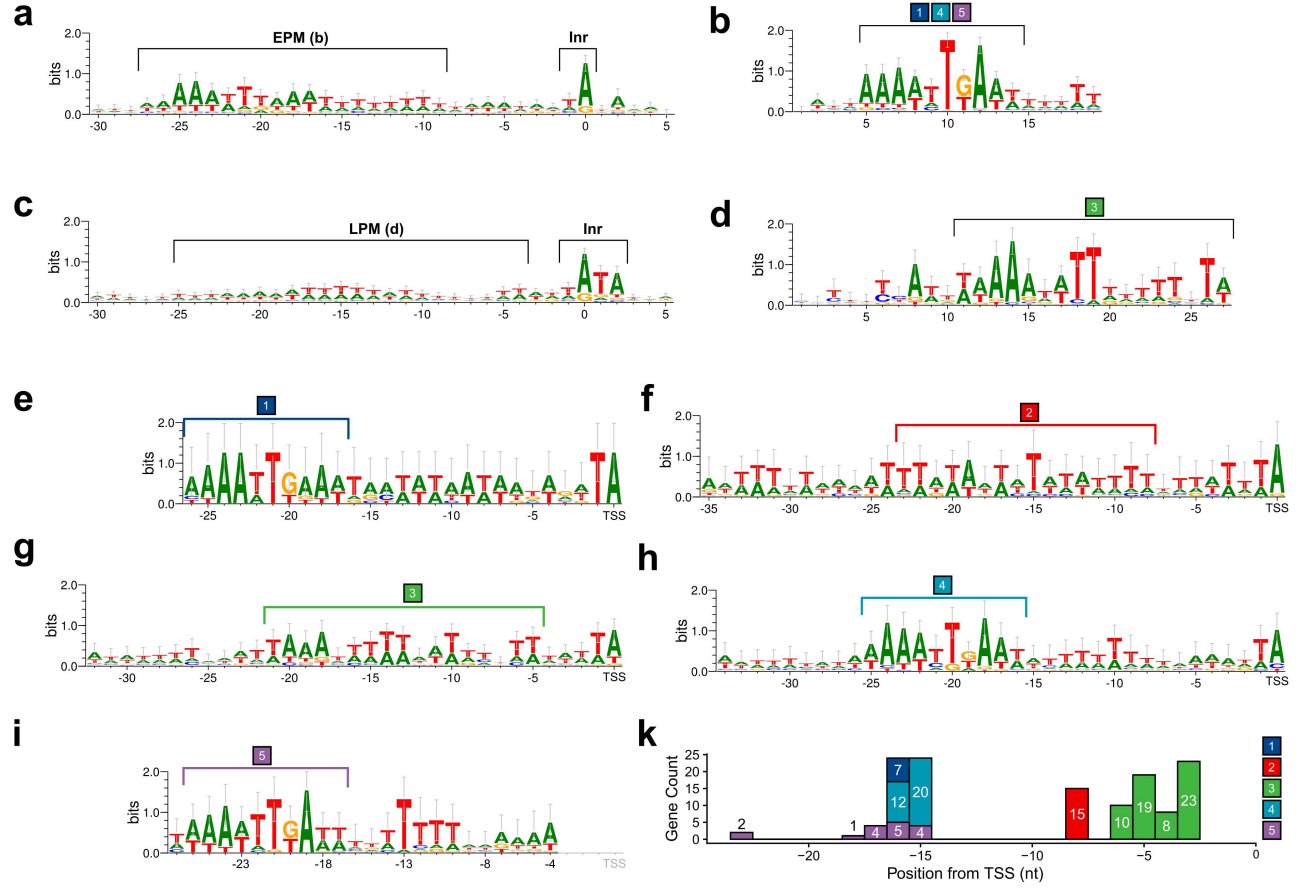


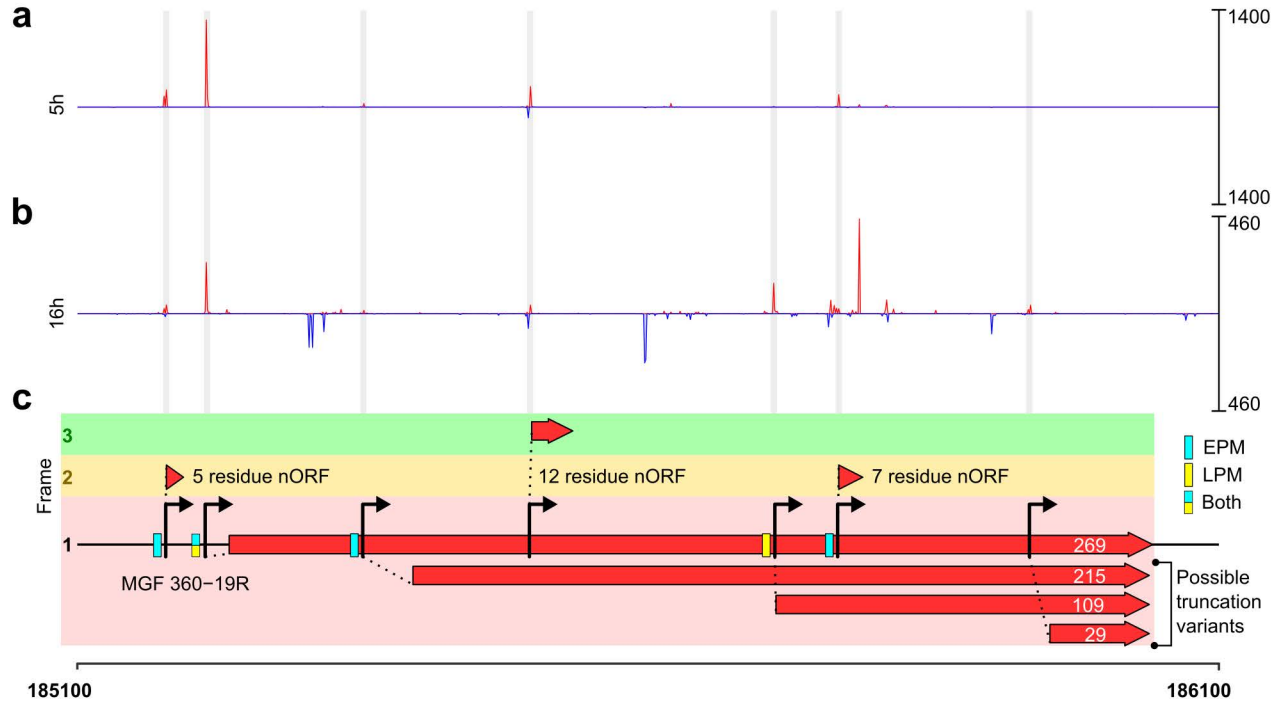


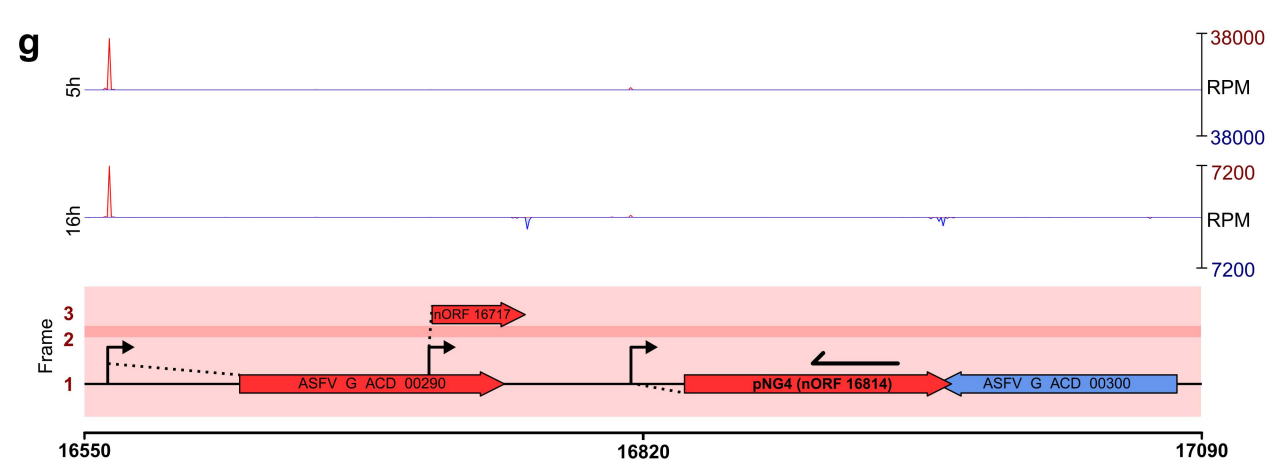
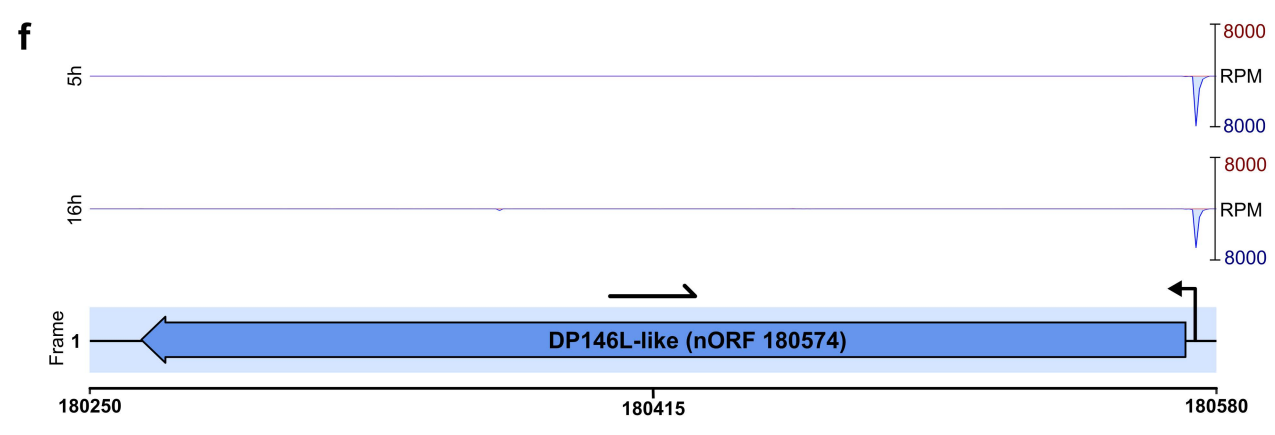
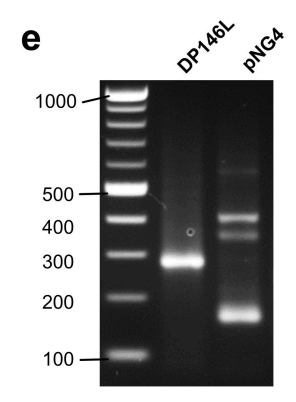
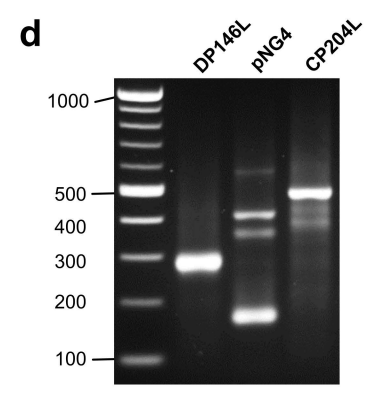
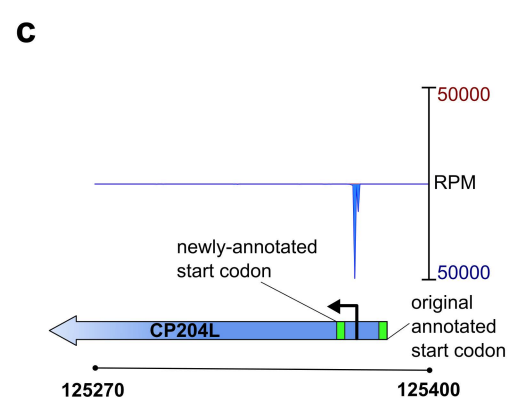
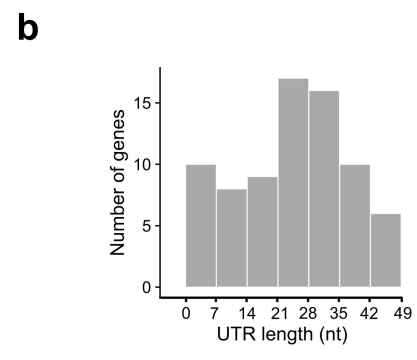
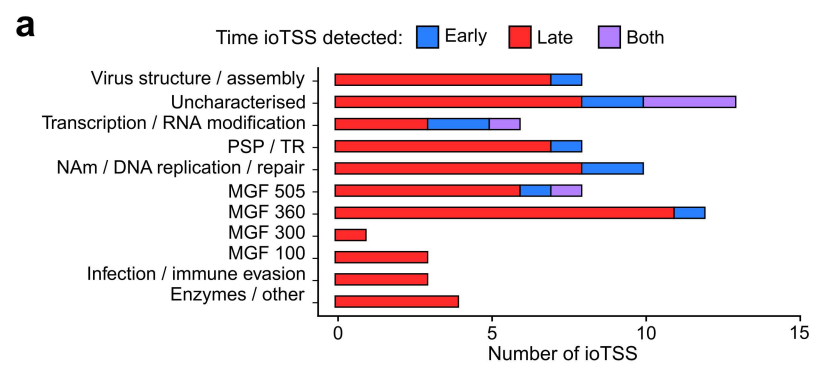








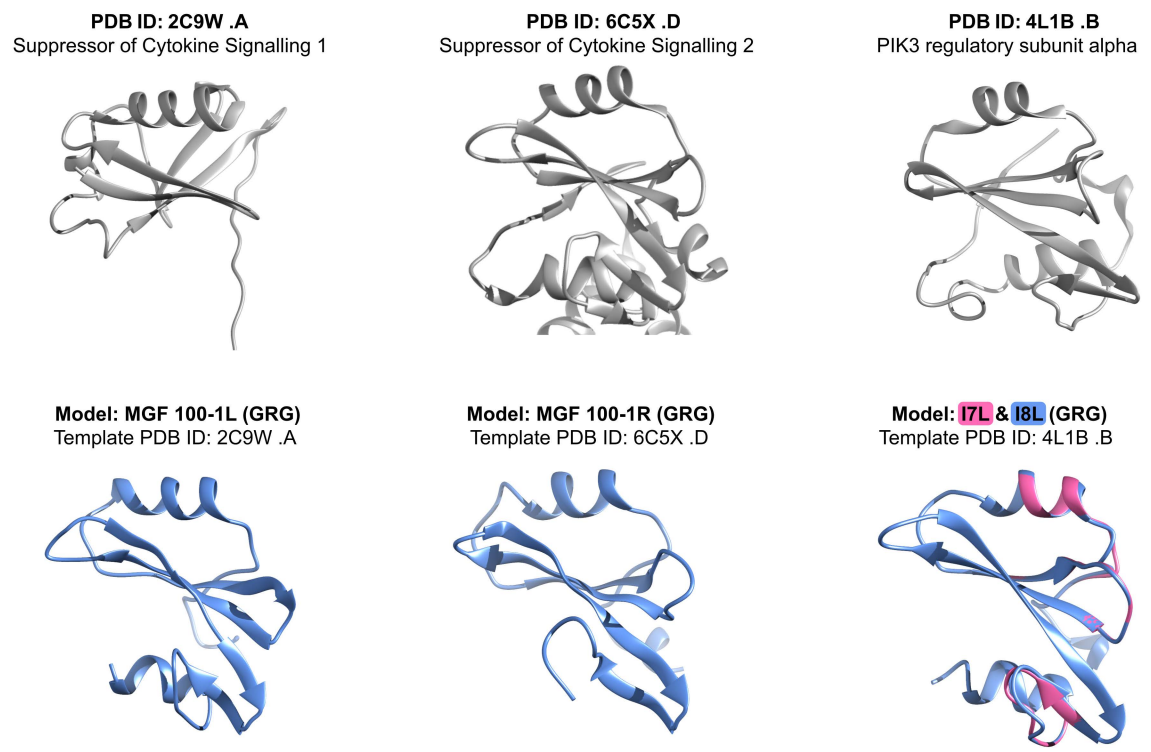




a

Genotype	ASFV strain	Pathogenic	Source	1R	1L/2L (DP141L)	3L (DP146L)	I7L	I8L
I	BA71V	N	NC_001659.2		←	←		
I	BA71	Y	NC_044942	//	←	←	←	←
I	Portugal, OURT88/3	N	AM712240.1	→	//	←	←	←
I	Benin 97/1	Y	AM712239.1		←	←	←	←
II	Georgia 2007/1	Y	FR682468.2	→	//	←	←	←
II	Georgia 2007/1-VP110	N	Krug <i>et al.</i>	→	//	←		
II	China/2018/AnhuiXCGQ	Y	MK128995.1	→	//	←	←	←
IX	Ken05/Tk1	Y	KM111294.1	→	//	←	←	←
X	Kenya 1950	Y	AY261360.1	→	//	←	←	←

b



c

